

# Dynamic Critical Behavior of the Swendsen–Wang Algorithm for the Three-Dimensional Ising Model

Giovanni Ossola  
Alan D. Sokal  
*Department of Physics*  
*New York University*  
*4 Washington Place*  
*New York, NY 10003 USA*  
GIOVANNI.OSSOLA@PHYSICS.NYU.EDU, SOKAL@NYU.EDU

February 12, 2004

## Abstract

We have performed a high-precision Monte Carlo study of the dynamic critical behavior of the Swendsen–Wang algorithm for the three-dimensional Ising model at the critical point. For the dynamic critical exponents associated to the integrated autocorrelation times of the “energy-like” observables, we find  $z_{\text{int},\mathcal{N}} = z_{\text{int},\mathcal{E}} = z_{\text{int},\mathcal{E}'} = 0.459 \pm 0.005 \pm 0.025$ , where the first error bar represents statistical error (68% confidence interval) and the second error bar represents possible systematic error due to corrections to scaling (68% subjective confidence interval). For the “susceptibility-like” observables, we find  $z_{\text{int},\mathcal{M}^2} = z_{\text{int},\mathcal{S}_2} = 0.443 \pm 0.005 \pm 0.030$ . For the dynamic critical exponent associated to the exponential autocorrelation time, we find  $z_{\text{exp}} \approx 0.481$ . Our data are consistent with the Coddington–Baillie conjecture  $z_{\text{SW}} = \beta/\nu \approx 0.5183$ , especially if it is interpreted as referring to  $z_{\text{exp}}$ .

**PACS codes:** 05.50.+q, 05.10.Ln, 64.60.Cn, 64.60.Ht.

**Key Words:** Ising model; Potts model; Swendsen–Wang algorithm; cluster algorithm; Monte Carlo; autocorrelation time; dynamic critical exponent.

# 1 Introduction

Monte Carlo (MC) simulations [1–7] have become a standard and powerful tool for gaining nonperturbative insights into statistical-mechanical systems and lattice field theories. However, their practical success is severely limited by critical slowing-down: the autocorrelation time  $\tau$  — that is, roughly speaking, the time needed to produce one “statistically independent” configuration — diverges near a critical point. More precisely, for a finite system of linear size  $L$  at criticality, we expect a behavior  $\tau \sim L^z$  for large  $L$ . The power  $z$  is a *dynamic critical exponent*, and it depends on both the system and the Monte Carlo algorithm.

Local Monte Carlo algorithms (such as single-site Metropolis or heat bath) generally have a dynamic critical exponent  $z \gtrsim 2$ . This makes it very hard to get high-precision data very close to the critical point on large lattices.

In some cases, a much better dynamical behavior can be obtained by including non-local moves, such as cluster flips.<sup>1</sup> In particular, the Swendsen–Wang (SW) cluster algorithm [9] for the ferromagnetic  $q$ -state Potts model achieves a significant reduction in  $z$  compared to the local algorithms: one has  $z$  between 0 and 1, where the exact value depends on  $q$  and on the dimensionality of the lattice. The most favorable case is the two-dimensional (2D) Ising model ( $q = 2$ ), for which the best currently available numerical estimate is  $z = 0.222 \pm 0.007$  [10] (see also the discussion below). In other cases, the performance of the SW algorithm is somewhat less impressive but still quite good: e.g.,  $z = 0.514 \pm 0.006$  for the 2D 3-state Potts model [11],  $z \approx 1$  for the 2D 4-state Potts model [12, 13],  $z \approx 0.45$ – $0.75$  for the 3D Ising model [9, 14–20], and  $z \approx 0.86$ – $1$  for the 4D Ising model [16, 21–24]. Clearly, we would like to understand why the SW algorithm works so well in some cases and less well in others. We hope in this way to obtain new insights into the dynamics of non-local Monte Carlo algorithms, with the ultimate aim of devising new and more efficient algorithms.

There is at present no adequate theory for predicting the dynamic critical behavior of an SW-type algorithm. However, Li and Sokal [25] have proven that the autocorrelation times of the Swendsen–Wang algorithm for the  $q$ -state Potts ferromagnet are *bounded below* by a multiple of the specific heat:

$$\tau_{\text{int}, \mathcal{N}}, \tau_{\text{int}, \mathcal{E}}, \tau_{\text{int}, \mathcal{E}'}, \tau_{\text{exp}} \geq \text{const} \times C_H . \quad (1.1)$$

Here  $\mathcal{N}$  is the bond occupation in the SW algorithm,  $\mathcal{E}$  is the energy,  $\mathcal{E}'$  is the nearest-neighbor connectivity, and  $C_H$  is the specific heat;  $\tau_{\text{int}}$  and  $\tau_{\text{exp}}$  denote the integrated and exponential autocorrelation times, respectively [4]. As a result one has for the dynamic critical exponents

$$z_{\text{int}, \mathcal{N}}, z_{\text{int}, \mathcal{E}}, z_{\text{int}, \mathcal{E}'}, z_{\text{exp}} \geq \alpha/\nu , \quad (1.2)$$

where  $\alpha$  and  $\nu$  are the standard *static* critical exponents. Thus, the SW algorithm cannot *completely* eliminate the critical slowing-down if the specific heat is divergent at criticality.<sup>2</sup>

---

<sup>1</sup>See [4, 8] for reviews of collective-mode Monte Carlo methods.

<sup>2</sup>The bound (1.1)/(1.2) has also been proven to hold [12] for the direct SW-type algorithm [26] for the Ashkin–Teller (AT) model [27, 28], which interpolates between the 2-state (Ising) and 4-state Potts models.

The physical mechanism underlying the Li–Sokal proof is the slow evolution of the bond occupation  $\mathcal{N}$ : its mean-square change per SW iteration is of order  $V$  (volume), while its variance in the equilibrium distribution is of order  $VC_H$ ; this leads to (1.1). In addition, Salas and Sokal [11] have proven, under a very mild and eminently plausible condition<sup>3</sup>, that all three “energy-like” observables have the same dynamic critical exponent:

$$z_{\text{int},\mathcal{N}} = z_{\text{int},\mathcal{E}} = z_{\text{int},\mathcal{E}'} . \quad (1.3)$$

For details on all these results, see [11, Section 2.2].

One important question is whether the Li–Sokal bound (1.1)/(1.2) is sharp or not. An affirmative answer would imply that we could use the bound to predict the dynamic critical exponent(s)  $z$  given only the static critical exponents of the system. There are three possibilities:

- i) The bound (1.1) is *sharp* (i.e., the ratio  $\tau/C_H$  is bounded), so that (1.2) is an *equality*.
- ii) The bound is *sharp modulo a logarithm* (i.e.,  $\tau/C_H \sim \log^p L$  for  $p > 0$ ).
- iii) The bound is *not sharp* (i.e.,  $\tau/C_H \sim L^p$  for  $p > 0$ ), so that (1.2) is a *strict inequality*.

The best currently available data concern the two-dimensional Potts models with  $q = 2, 3, 4$ , for which we have

$$\begin{aligned} q = 2: \quad \alpha/\nu &= 0 (\times \log) & z_{\text{int},\mathcal{E}'} &= 0.222 \pm 0.007 \text{ [10]} \\ q = 3: \quad \alpha/\nu &= 2/5 & z_{\text{int},\mathcal{E}'} &= 0.514 \pm 0.006 \text{ [11]} \\ q = 4: \quad \alpha/\nu &= 1 (\times \log^{-3/2}) & z_{\text{int},\mathcal{E}} &= 0.876 \pm 0.011 \text{ [13]} \end{aligned}$$

Here the values of  $\alpha/\nu$  are exact [13, 29, 30], while the values of  $z$  are the best available numerical estimates from pure power-law fits. Note, however, that the estimate of  $z$  for  $q = 4$  *cannot* be correct, as it violates the Li–Sokal bound (1.2); presumably it is corrupted by the same multiplicative logarithmic corrections that afflict the specific heat.<sup>4</sup> For this reason, the papers [10, 11, 13] analyzed also the ratio  $\tau/C_H$  in order to test directly the sharpness of the Li–Sokal bound. It was found that the data for  $q = 2, 3, 4$  are consistent with two scenarios: either the Li–Sokal bound is non-sharp by a very small power ( $p \approx 0.06$ – $0.12$ ), or else it is sharp modulo a logarithm (possibly with power  $p = 1$ ). Not surprisingly, it is exceedingly difficult to distinguish numerically between these two scenarios.

For the three- and four-dimensional Ising models, by contrast, the Li–Sokal bound (1.2) is clearly *not* sharp: the numerical estimates of  $z$  are much larger than  $\alpha/\nu$ . It follows that another physical mechanism, beyond the one captured in the Li–Sokal proof, must be principally responsible for the critical slowing-down in these cases; but it is far from clear what this mechanism is. A natural first step towards identifying this mechanism would be to obtain accurate numerical estimates for  $z$  in the three- and four-dimensional Ising models.

---

<sup>3</sup>The condition is that the normalized autocorrelation functions of the bond occupation at time lags 1 and 2, i.e.  $\rho_{\mathcal{N}\mathcal{N}}(1)$  and  $\rho_{\mathcal{N}\mathcal{N}}(2)$ , should be bounded away from zero as the lattice size  $L$  tends to infinity.

<sup>4</sup>Indeed, a pure power-law fit to the Monte Carlo data for the specific heat yielded  $\alpha/\nu = 0.770 \pm 0.008$  [13].

Unfortunately, the numerical results in the four-dimensional case are almost nonexistent<sup>5</sup>, and in the three-dimensional case are wildly contradictory. In chronological order, the results for the three-dimensional Ising model are as follows:

- 1987:  $z_{\text{exp},\mathcal{E}} = 0.75 \pm 0.01$ , based on unspecified lattice sizes [9]
- 1989:  $z_{\text{int},\mathcal{E}} = z_{\text{int},\mathcal{M}^2} = 0.50 \pm 0.03$ , based on  $L \leq 64$  [14]
- 1990:  $z_{\text{exp},\mathcal{C}_1} = 0.46 \pm 0.01$  ( $\mathcal{C}_1$  = size of the largest cluster), based on  $L \leq 89$  extrapolated to  $L = \infty$  [15]<sup>6</sup>
- 1992:  $z_{\text{int},\mathcal{E}} = 0.54 \pm 0.02$ , based on  $L \leq 48$  [16]
- 1993:  $z_{\text{exp}} = 0.61 \pm 0.02$ ,  $z_{\text{int},\mathcal{E}} = 0.58 \pm 0.02$ ,  $z_{\text{int},\mathcal{M}^2} = 0.57 \pm 0.02$  and  $z_{\text{int},|\mathcal{M}|} = 0.55 \pm 0.02$ , based on  $L \leq 32$  [18]
- 1993:  $z_{\text{int},\mathcal{E}} = 0.49 \pm 0.02$  and  $z_{\text{int},|\mathcal{M}|} = 0.48 \pm 0.01$ , based on  $L \leq 60$  [19]
- 2002:  $z_{\text{int},\mathcal{E}} \approx 0.50$ , based on  $L \leq 128$  [20]<sup>7</sup>

The reason for the discrepancies is unclear, but there does seem to be a tendency for the estimates of  $z$  to decrease as larger lattices are used — an effect that could easily be understood as arising from corrections to scaling.

The purpose of this paper is to restudy the dynamic critical behavior of the SW algorithm for the three-dimensional Ising model, using much larger lattices (up to  $L = 256$ ), vastly higher statistics (well over  $10^7$  SW iterations at each lattice size), and a careful finite-size-scaling analysis. For the dynamic critical exponents associated to the integrated autocorrelation times of the “energy-like” observables, we find

$$z_{\text{int},\mathcal{N}} = z_{\text{int},\mathcal{E}} = z_{\text{int},\mathcal{E}'} = 0.459 \pm 0.005 \pm 0.025, \quad (1.4)$$

where the first error bar represents statistical error (68% confidence interval) and the second error bar represents possible systematic error due to corrections to scaling (68% subjective

---

<sup>5</sup>The only numerical study of which we are aware is [16], which yielded  $z_{\text{int},\mathcal{E}} = 0.86 \pm 0.02$ , based on lattices of size  $4 \leq L \leq 16$  (which by present-day standards are much too small). In addition, there have been numerical [22, 23] and analytic [22–24] studies of the Swendsen–Wang algorithm for the Ising ferromagnet on the complete graph (also known as the Curie–Weiss or “mean-field” model), which indicate  $z = 1$ . This model is *presumed* to lie in the same dynamic universality class as the Ising model on a regular lattice of dimension  $d \geq 4$ , but high-precision numerical tests of this quite plausible conjecture are lacking.

<sup>6</sup>Wang [15] also studied the magnetization (including sign) of the largest cluster in a variant of the Swendsen–Wang algorithm in which the largest cluster is not flipped. But it is far from clear whether this observable corresponds to *any* observable in the standard Swendsen–Wang algorithm. Indeed, Wang found that the exponential autocorrelation time of this observable is several times *larger* than that of  $\mathcal{C}_1$ . And since there is good reason to believe (see Section 5.2 below) that  $\mathcal{C}_1$  does indeed have a significant overlap with the slowest mode in the Swendsen–Wang algorithm, this suggests that Wang’s observable is *not* interpretable within the standard Swendsen–Wang algorithm, but rather represents a *new* slow mode in the variant algorithm.

<sup>7</sup>A pure power-law fit to the raw data of Wang, Kozan and Swendsen [20] yields a decent  $\chi^2$  if (and only if)  $L_{\text{min}} \geq 32$ . Our preferred fit is  $L_{\text{min}} = 32$ , and yields  $z_{\text{int},\mathcal{E}} = 0.502 \pm 0.012$  ( $\chi^2 = 0.440$ , 1 DF, level = 50.7%). We thank Jian-Sheng Wang for supplying us with these raw data.

confidence interval). For the “susceptibility-like” observables, we find

$$z_{\text{int},\mathcal{M}^2} = z_{\text{int},\mathcal{S}_2} = 0.443 \pm 0.005 \pm 0.030 . \quad (1.5)$$

Finally, for the dynamic critical exponent associated to the exponential autocorrelation time, we obtain the rough estimate

$$z_{\text{exp}} \approx 0.481 . \quad (1.6)$$

It is possible that some or all of these exponents are in fact exactly equal.

The present paper is organized as follows: Section 2 reviews the basics of the Swendsen–Wang algorithm and the definitions of autocorrelation times and observables. In Section 3 we discuss our methods of statistical data analysis. In Section 4 we summarize our Monte Carlo simulations. In Section 5 we present the analysis of our dynamic data. In Section 6 we discuss our results in the light of various conjectures that have been made by previous workers. The static data from our simulations will be analyzed in a separate paper [31].

## 2 Basic set-up and notation

### 2.1 Potts model and Swendsen–Wang algorithm

The  $q$ -state Potts model assigns to each lattice site  $i$  a spin variable  $\sigma_i$  taking values in the set  $\{1, 2, \dots, q\}$ ; these spins interact through the reduced Hamiltonian

$$\mathcal{H}_{\text{Potts}} = -\beta \sum_{\langle ij \rangle} (\delta_{\sigma_i, \sigma_j} - 1) , \quad (2.1)$$

where the sum runs over all the nearest-neighbor pairs  $\langle ij \rangle$  (each pair counted once). To simplify the notation we shall henceforth write  $\delta_{\sigma_i, \sigma_j} \equiv \delta_{\sigma_b}$  for a bond  $b = \langle ij \rangle$ . The ferromagnetic case corresponds to  $\beta \geq 0$ . The partition function is defined as

$$Z = \sum_{\{\sigma\}} e^{-\mathcal{H}} = \sum_{\{\sigma\}} \exp \left[ \beta \sum_b (\delta_{\sigma_b} - 1) \right] . \quad (2.2)$$

Finally, the Boltzmann weight of a configuration  $\{\sigma\}$  is given by

$$W_{\text{Potts}}(\{\sigma\}) = \frac{1}{Z} \exp \left[ \beta \sum_b (\delta_{\sigma_b} - 1) \right] = \frac{1}{Z} \prod_b (1 - p + p \delta_{\sigma_b}) \quad (2.3)$$

where  $p = 1 - e^{-\beta}$ .

The idea behind the Swendsen–Wang (SW) algorithm [9, 32] is to decompose the Boltzmann weight (2.3) by introducing new dynamical variables  $n_b = 0, 1$  living on the bonds of the lattice, and to simulate the joint model of old and new variables by alternately updating one set of variables conditional on the other set. The Boltzmann weight of the joint model is

$$W_{\text{joint}}(\{\sigma\}, \{n\}) = \frac{1}{Z} \prod_b [(1 - p) \delta_{n_b, 0} + p \delta_{\sigma_b} \delta_{n_b, 1}] . \quad (2.4)$$

The marginal distribution of (2.4) with respect to the spin variables reproduces the Potts-model Boltzmann weight (2.3). The marginal distribution of (2.4) with respect to the bond variables is the Fortuin–Kasteleyn [33–35] random-cluster model with parameter  $q$ :

$$W_{\text{RC}}(\{n\}) = \frac{1}{Z} \left[ \prod_{b: n_b=1} p \right] \left[ \prod_{b: n_b=0} (1-p) \right] q^{\mathcal{C}(\{n\})} \quad (2.5)$$

where  $\mathcal{C}(\{n\})$  is the number of connected components (including one-site components) in the graph whose edges are the bonds with  $n_b = 1$ .

We can also consider the conditional probabilities of the joint distribution (2.4). The conditional distribution of the  $\{n\}$  given the  $\{\sigma\}$  is as follows: independently for each bond  $b = \langle ij \rangle$ , one sets  $n_b = 0$  when  $\sigma_i \neq \sigma_j$ , and sets  $n_b = 0$  and  $1$  with probabilities  $1-p$  and  $p$  when  $\sigma_i = \sigma_j$ . Finally, the conditional distribution of the  $\{\sigma\}$  given the  $\{n\}$  is as follows: independently for each connected cluster, one sets all the spins  $\sigma_i$  in that cluster equal to the same value, chosen with uniform probability from the set  $\{1, 2, \dots, q\}$ .

The Swendsen–Wang algorithm simulates the joint probability distribution (2.4) by alternately applying the two conditional distributions just described. That is, we first erase the current  $\{n\}$  configuration, and generate a new  $\{n\}$  configuration from the conditional distribution given  $\{\sigma\}$ ; we then erase the current  $\{\sigma\}$  configuration, and generate a new  $\{\sigma\}$  configuration from the conditional distribution given  $\{n\}$ . A single step of the SW algorithm consists of these two “half-steps”.

## 2.2 Autocorrelation functions and autocorrelation times

Let  $\mathcal{O}$  be any observable (i.e. any function of  $\{\sigma\}$  and  $\{n\}$ ), and let  $\mathcal{O}(t)$  be its evolution in Monte Carlo time (where one unit of time corresponds to a single step of the Swendsen–Wang algorithm). The unnormalized autocorrelation function associated to the observable  $\mathcal{O}$  is defined as

$$C_{\mathcal{O}\mathcal{O}}(t) \equiv \langle \mathcal{O}(s)\mathcal{O}(s+t) \rangle - \langle \mathcal{O} \rangle^2, \quad (2.6)$$

where the expectations are taken *in equilibrium*. The corresponding normalized autocorrelation function is defined as

$$\rho_{\mathcal{O}\mathcal{O}}(t) \equiv \frac{C_{\mathcal{O}\mathcal{O}}(t)}{C_{\mathcal{O}\mathcal{O}}(0)} = \frac{C_{\mathcal{O}\mathcal{O}}(t)}{\text{var}(\mathcal{O})}. \quad (2.7)$$

The integrated and exponential autocorrelation times associated to the observable  $\mathcal{O}$  are defined as<sup>8</sup>

$$\tau_{\text{int},\mathcal{O}} = \frac{1}{2} \sum_{t=-\infty}^{\infty} \rho_{\mathcal{O}\mathcal{O}}(t) \quad (2.8)$$

---

<sup>8</sup>For a general Markov chain, the “lim” in (2.9) should strictly speaking be replaced by “lim sup”, and  $\rho_{\mathcal{O}\mathcal{O}}(t)$  should be replaced by its absolute value. But in the Swendsen–Wang algorithm it can be *proven* that the limit really exists, and that  $\rho_{\mathcal{O}\mathcal{O}}(t) \geq 0$  for all  $t$ ; this follows from the spectral representation [25] [11, Section 2.2].

$$\tau_{\text{exp},\mathcal{O}} = \lim_{|t| \rightarrow \infty} \frac{-|t|}{\log \rho_{\mathcal{O}\mathcal{O}}(t)} \quad (2.9)$$

Finally, the exponential autocorrelation time of the system is defined as

$$\tau_{\text{exp}} = \sup_{\mathcal{O}} \tau_{\text{exp},\mathcal{O}} , \quad (2.10)$$

where the supremum is taken over all observables  $\mathcal{O}$ . This autocorrelation time measures the decay rate of the slowest mode of the system. All observables that are not orthogonal to this slowest mode satisfy  $\tau_{\text{exp},\mathcal{O}} = \tau_{\text{exp}}$ .

It is important to remember that there is not just one autocorrelation time, but many: namely,  $\tau_{\text{exp}}$  as well as  $\tau_{\text{int},\mathcal{O}}$  for each observable  $\mathcal{O}$ . In all but the most trivial Markov chains, these autocorrelation times are *not* equal. Correspondingly, there are many dynamic critical exponents: namely,  $z_{\text{exp}}$  as well as  $z_{\text{int},\mathcal{O}}$  for each observable  $\mathcal{O}$ . These exponents *may* in some cases be equal (i.e., the corresponding autocorrelation times may scale proportionally as the critical point is approached), but they need not be; this is a detailed dynamical question, and the answer will vary from model to model.

## 2.3 Observables to be measured

As just explained, the Swendsen–Wang algorithm is most naturally defined in the general context of the  $q$ -state Potts ferromagnet. It is therefore most convenient and natural to use a formalism that is valid for arbitrary  $q$ ; at the end we can specialize to the Ising case  $q = 2$ .

The nicest “geometric” representation of Potts spins is the *hypertetrahedral representation*, defined as follows: Let  $\{\mathbf{e}^{(\alpha)}\}_{\alpha=1}^q$  be unit vectors in  $\mathbb{R}^{q-1}$  satisfying  $\mathbf{e}^{(\alpha)} \cdot \mathbf{e}^{(\beta)} = (q\delta^{\alpha\beta} - 1)/(q - 1)$ . Geometrically, these vectors point from the center to the vertices of a unit hypertetrahedron in  $\mathbb{R}^{q-1}$ . We then represent a Potts spin  $\sigma_x \in \{1, 2, \dots, q\}$  by the unit vector  $\boldsymbol{\sigma}_x \equiv \mathbf{e}^{(\sigma_x)}$  in  $\mathbb{R}^{q-1}$ . This representation captures the  $S_q$  (permutation group) symmetry of the Potts Hamiltonian (2.1), and for  $q = 2$  it reduces to the usual representation of Ising spins  $\sigma_x = \pm 1$ . We have in particular

$$\boldsymbol{\sigma}_x \cdot \boldsymbol{\sigma}_y = \frac{q\delta_{\sigma_x, \sigma_y} - 1}{q - 1} , \quad (2.11)$$

so that the Potts Hamiltonian can be written equivalently as

$$\mathcal{H} = -\beta_{\text{Potts}} \sum_{\langle ij \rangle} \delta_{\sigma_i, \sigma_j} + \text{const} \quad (2.12a)$$

$$= -\beta_{\text{tetr}} \sum_{\langle ij \rangle} \boldsymbol{\sigma}_i \cdot \boldsymbol{\sigma}_j + \text{const} \quad (2.12b)$$

where

$$\beta_{\text{tetr}} = \frac{q - 1}{q} \beta_{\text{Potts}} . \quad (2.13)$$

For  $q = 2$  this yields  $\beta_{\text{Ising}} = \beta_{\text{Potts}}/2$ , where  $\beta_{\text{Ising}} \equiv \beta_{\text{tetr}}$  corresponds to the usual Ising normalization for the inverse temperature.

Let us now consider the  $q$ -state Potts ferromagnet on a  $d$ -dimensional periodic hypercubic lattice of linear size  $L$ . We write  $V = L^d$  for the number of sites, and  $B = dL^d$  for the number of bonds. We shall consider the following observables:

- (minus) the total energy

$$\mathcal{E} \equiv \sum_{\langle xy \rangle} \boldsymbol{\sigma}_x \cdot \boldsymbol{\sigma}_y \quad (2.14a)$$

$$= \sum_{\langle xy \rangle} \frac{q \delta_{\sigma_x, \sigma_y} - 1}{q - 1} \quad (2.14b)$$

where the sum runs over all the nearest-neighbor pairs  $\langle xy \rangle$  (each pair counted once).

- the bond occupation

$$\mathcal{N} \equiv \sum_{\langle xy \rangle} n_{xy} \quad (2.15)$$

- the nearest-neighbor connectivity (which is an energy-like observable [11])

$$\mathcal{E}' \equiv \sum_{\langle xy \rangle} \gamma_{xy} , \quad (2.16)$$

where  $\gamma_{xy}$  equals 1 if both ends of the bond  $\langle xy \rangle$  belong to the same cluster, and 0 otherwise. More generally, the connectivity  $\gamma_{ij}$  can be defined for an arbitrary pair  $i, j$  of sites:

$$\gamma_{ij}(\{n\}) = \begin{cases} 1 & \text{if } i \text{ is connected to } j \\ 0 & \text{if } i \text{ is not connected to } j \end{cases} \quad (2.17)$$

We shall also use higher connectivities, such as

$$\gamma_{ijkl}(\{n\}) = \begin{cases} 1 & \text{if } i, j, k, l \text{ are all connected together} \\ 0 & \text{otherwise} \end{cases} \quad (2.18)$$

- the squared magnetization

$$\mathcal{M}^2 = \left( \sum_x \boldsymbol{\sigma}_x \right)^2 \quad (2.19a)$$

$$= \frac{q}{q-1} \sum_{\alpha=1}^q \left( \sum_x \delta_{\sigma_x, \alpha} \right)^2 - \frac{V^2}{q-1} \quad (2.19b)$$

- higher powers of the magnetization

$$\mathcal{M}^{2n} = (\mathcal{M}^2)^n \quad (2.20)$$

(In this paper, we measured only  $\mathcal{M}^2$  and  $\mathcal{M}^4$ .)



- the square of the Fourier transform of the spin variable at the smallest allowed non-zero momentum

$$\mathcal{F} = \frac{1}{d} \sum_{j=1}^d \left| \sum_x \sigma_x e^{2\pi i x_j / L} \right|^2 \quad (2.21a)$$

$$= \frac{q}{q-1} \times \frac{1}{d} \sum_{j=1}^d \sum_{\alpha=1}^q \left| \sum_x \delta_{\sigma_x, \alpha} e^{2\pi i x_j / L} \right|^2 \quad (2.21b)$$

where  $(x_1, x_2, \dots, x_d)$  are the Cartesian coordinates of point  $x$ . Note that  $\mathcal{F}$  is normalized to be comparable to its zero-momentum analogue  $\mathcal{M}^2$ .

- the number of clusters (= connected components) and the mean-square and mean-fourth-power size of the clusters

$$\mathcal{C} = \mathcal{S}_0 = \sum_C 1 \quad (2.22)$$

$$\mathcal{S}_2 = \sum_C \#(C)^2 = \sum_{x,y} \gamma_{xy} \quad (2.23)$$

$$\mathcal{S}_4 = \sum_C \#(C)^4 = \sum_{x,y,u,v} \gamma_{xyuv} \quad (2.24)$$

where the sum runs over all the clusters  $C$  of activated bonds, and  $\#(C)$  is the number of sites in the cluster  $C$ .

- the size  $\mathcal{C}_i$  of the  $i$ th largest cluster ( $\mathcal{C}_1 \geq \mathcal{C}_2 \geq \mathcal{C}_3 \geq \dots$ ). In this work we measured only  $\mathcal{C}_1$ ,  $\mathcal{C}_2$  and  $\mathcal{C}_3$ .

From these observables we compute the following expectation values:

- (minus) the energy density  $E$  per bond

$$E = \frac{1}{B} \langle \mathcal{E} \rangle, \quad (2.25)$$

where  $B = dV$  is the number of bonds in the lattice, so that a perfectly disordered (resp. ferromagnetically ordered) state has  $E = 0$  (resp.  $E = 1$ )

- the specific heat per bond

$$C_H = \frac{1}{B} \text{var}(\mathcal{E}) \equiv \frac{1}{B} [\langle \mathcal{E}^2 \rangle - \langle \mathcal{E} \rangle^2] \quad (2.26)$$

- the magnetic susceptibility

$$\chi = \frac{1}{V} \langle \mathcal{M}^2 \rangle \quad (2.27)$$

- the correlation function at momentum  $(2\pi/L, 0, \dots, 0)$

$$F = \frac{1}{V} \langle \mathcal{F} \rangle \quad (2.28)$$

- the second-moment correlation length

$$\xi = \frac{1}{2 \sin(\pi/L)} \left( \frac{\chi}{F} - 1 \right)^{1/2} \quad (2.29)$$

- the mean number of clusters

$$S_0 = \langle \mathcal{S}_0 \rangle \quad (2.30)$$

- the mean size of the  $i$ th largest cluster

$$C_i = \langle \mathcal{C}_i \rangle \quad (2.31)$$

For each observable  $\mathcal{O}$  discussed above, we have measured its autocorrelation function  $\rho_{\mathcal{O}\mathcal{O}}(t)$  and have used this to estimate the corresponding integrated autocorrelation time  $\tau_{\text{int},\mathcal{O}}$ . In Section 3 we explain how we derived estimates of the mean values and the error bars for both static and dynamic quantities.

**Remarks.** 1. Using the Fortuin–Kasteleyn identities [4, 33–35], which arise from the formulae for conditional expectations in the joint measure (2.4), it is not difficult to show that

$$\langle n_{xy} \rangle = p \langle \delta_{\sigma_x, \sigma_y} \rangle \quad (2.32)$$

$$\langle \sigma_x \cdot \sigma_y \rangle = \langle \gamma_{xy} \rangle \quad (2.33)$$

$$\langle \sigma_x \cdot \sigma_y \sigma_u \cdot \sigma_v \rangle = \left\langle \gamma_{xy} \gamma_{uv} + \frac{1}{q-1} (\gamma_{xu} \gamma_{yv} + \gamma_{xv} \gamma_{yu} - 2\gamma_{xyuv}) \right\rangle \quad (2.34)$$

and hence that

$$\langle \mathcal{N} \rangle = p \frac{(q-1)\langle \mathcal{E} \rangle + B}{q} \quad (2.35)$$

$$\langle \mathcal{E} \rangle = \langle \mathcal{E}' \rangle \quad (2.36)$$

$$\langle \mathcal{M}^2 \rangle = \langle \mathcal{S}_2 \rangle \quad (2.37)$$

$$\langle \mathcal{M}^4 \rangle = \frac{q+1}{q-1} \langle \mathcal{S}_2^2 \rangle - \frac{2}{q-1} \langle \mathcal{S}_4 \rangle \quad (2.38)$$

where  $p = 1 - e^{-\beta_{\text{Potts}}}$  is the Swendsen–Wang bond probability and  $B = dL^d$  is the number of bonds in the lattice. As a check on the correctness of our simulations, we have tested these identities to high precision, in the following way: Instead of comparing directly the left and right sides of each equation, which are strongly positively correlated in the Monte Carlo

simulation, a more sensitive test is to define new observables corresponding to the differences (i.e.,  $\mathcal{E} - \mathcal{E}'$  and so forth). Each such observable should have mean zero, and the error bars on the sample mean can be estimated using the standard error analysis outlined in Section 3 below. The comparison to zero yields the following  $\chi^2$  values:

$$\text{For (2.35): } \chi^2 = 160.95 \text{ (182 DF, level} = 87\%) \quad (2.39)$$

$$\text{For (2.36): } \chi^2 = 152.63 \text{ (182 DF, level} = 94\%) \quad (2.40)$$

$$\text{For (2.37): } \chi^2 = 188.28 \text{ (182 DF, level} = 36\%) \quad (2.41)$$

$$\text{For (2.38): } \chi^2 = 190.47 \text{ (182 DF, level} = 32\%) \quad (2.42)$$

Here we have treated each independent run (see Section 4) as a separate data point; DF means the number of degrees of freedom (i.e. the number of independent runs), and “level” means the confidence level of the fit (defined at the beginning of Section 5 below). The agreement is excellent.

2. As a further check on the correctness of our simulations, we have computed both sides of the identity

$$\rho_{\mathcal{N}\mathcal{N}}(1) = 1 - \frac{q^2 (1-p) E}{(q-1)^2 p C_H + q^2 (1-p) E} \quad (2.43)$$

proven in [25, equation 7] and [11, equation (2.16)].<sup>9</sup> This is a highly nontrivial test, as it relates static quantities (energy and specific heat) to a dynamic quantity (autocorrelation function of the bond occupation at time lag 1). We have also checked with great accuracy the identities [11]

$$C_{\mathcal{E}\mathcal{E}}(t) = \frac{1}{p^2} \left( \frac{q-1}{q} \right)^2 C_{\mathcal{N}\mathcal{N}}(t+1) \quad (2.44)$$

$$\rho_{\mathcal{E}\mathcal{E}}(t) = \frac{\rho_{\mathcal{N}\mathcal{N}}(t+1)}{\rho_{\mathcal{N}\mathcal{N}}(1)} \quad (2.45)$$

$$C_{\mathcal{E}'\mathcal{E}'}(t) = C_{\mathcal{E}\mathcal{E}}(t+1) \quad (2.46)$$

$$\rho_{\mathcal{E}'\mathcal{E}'}(t) = \frac{\rho_{\mathcal{E}\mathcal{E}}(t+1)}{\rho_{\mathcal{E}\mathcal{E}}(1)} \quad (2.47)$$

### 3 Statistical methods

In this paper we are aiming at extremely high precision for both static and dynamic quantities; and furthermore we need to disentangle the effects of statistical errors from the effects of systematic errors due to corrections to scaling. For this, it is essential to obtain accurate estimates not only of the static and dynamic quantities of interest, but also of their *error bars*: in this way we will be able (see Section 5) to perform  $\chi^2$  tests that provide an objective measure of the goodness of fit in each scaling Ansatz.

---

<sup>9</sup>Unfortunately, three different normalizations of the energy are used in [25], in [11], and in the present paper.

In this section we review briefly how we performed the statistical analysis of our raw Monte Carlo data. In particular, we describe how to compute the estimators for the mean value and the variance of both static and dynamic quantities. These methods are based on well-known results of time-series analysis [36, 37]. More details on the methods used here can be found in [38, Appendix C], [4, Section 3] and [11, Section 4].

Let us consider a generic observable  $\mathcal{O}$ , whose mean is equal to  $\mu_{\mathcal{O}}$ . Its corresponding unnormalized and normalized autocorrelation functions are denoted by  $C_{\mathcal{O}\mathcal{O}}(t) \equiv \langle \mathcal{O}(0)\mathcal{O}(t) \rangle - \langle \mathcal{O} \rangle^2$  and  $\rho_{\mathcal{O}\mathcal{O}}(t) \equiv C_{\mathcal{O}\mathcal{O}}(t)/C_{\mathcal{O}\mathcal{O}}(0)$ , respectively. We also define the integrated autocorrelation time

$$\tau_{\text{int},\mathcal{O}} = \frac{1}{2} \sum_{t=-\infty}^{\infty} \rho_{\mathcal{O}\mathcal{O}}(t) . \quad (3.1)$$

Given a sequence of  $n$  Monte Carlo measurements of the observable  $\mathcal{O}$  — call them  $\{\mathcal{O}_1, \dots, \mathcal{O}_n\}$  — the natural estimator of the mean  $\mu_{\mathcal{O}}$  is the sample mean

$$\overline{\mathcal{O}} \equiv \frac{1}{n} \sum_{i=1}^n \mathcal{O}_i . \quad (3.2)$$

This estimator is unbiased and has a variance

$$\text{var}(\overline{\mathcal{O}}) = \frac{1}{n^2} \sum_{r,s=1}^n C_{\mathcal{O}\mathcal{O}}(r-s) \quad (3.3a)$$

$$= \frac{1}{n} \sum_{t=-(n-1)}^{n-1} \left(1 - \frac{|t|}{n}\right) C_{\mathcal{O}\mathcal{O}}(t) \quad (3.3b)$$

$$\approx \frac{1}{n} 2\tau_{\text{int},\mathcal{O}} C_{\mathcal{O}\mathcal{O}}(0) \quad \text{for } n \gg \tau_{\text{int},\mathcal{O}} \quad (3.3c)$$

This means that the variance is a factor  $2\tau_{\text{int},\mathcal{O}}$  larger than it would be if the measurements were uncorrelated. It is, therefore, very important to estimate the autocorrelation time  $\tau_{\text{int},\mathcal{O}}$  in order to ensure a correct determination of the error bar on the (static) quantity  $\mu_{\mathcal{O}}$ .

The natural estimator for the unnormalized autocorrelation function  $C_{\mathcal{O}\mathcal{O}}(t)$  is

$$\hat{C}_{\mathcal{O}\mathcal{O}}(t) \equiv \frac{1}{n-|t|} \sum_{i=1}^{n-|t|} (\mathcal{O}_i - \mu_{\mathcal{O}})(\mathcal{O}_{i+|t|} - \mu_{\mathcal{O}}) \quad (3.4)$$

if the mean  $\mu_{\mathcal{O}}$  is known, and

$$\hat{\hat{C}}_{\mathcal{O}\mathcal{O}}(t) \equiv \frac{1}{n-|t|} \sum_{i=1}^{n-|t|} (\mathcal{O}_i - \overline{\mathcal{O}})(\mathcal{O}_{i+|t|} - \overline{\mathcal{O}}) \quad (3.5)$$

if the mean  $\mu_{\mathcal{O}}$  is unknown. We emphasize that, for each  $t$ , the estimators  $\hat{C}_{\mathcal{O}\mathcal{O}}(t)$  and  $\hat{\hat{C}}_{\mathcal{O}\mathcal{O}}(t)$  are *random variables* [in contrast to  $C_{\mathcal{O}\mathcal{O}}(t)$ , which is a *number*]. The estimator  $\hat{C}_{\mathcal{O}\mathcal{O}}(t)$  is unbiased, and  $\hat{\hat{C}}_{\mathcal{O}\mathcal{O}}(t)$  is biased by terms of order  $1/n$ . The covariance matrices of

$\widehat{C}_{\mathcal{O}\mathcal{O}}$  and  $\widehat{\widehat{C}}_{\mathcal{O}\mathcal{O}}$  are the same to leading order in the large- $n$  limit (i.e.,  $n \gg \tau_{\text{int},\mathcal{O}}$ ), and we have [36, 37]

$$\begin{aligned} \text{cov}(\widehat{C}_{\mathcal{O}\mathcal{O}}(t), \widehat{C}_{\mathcal{O}\mathcal{O}}(u)) &= \frac{1}{n} \sum_{i=-\infty}^{\infty} [C_{\mathcal{O}\mathcal{O}}(m)C_{\mathcal{O}\mathcal{O}}(m+u-t) + C_{\mathcal{O}\mathcal{O}}(m+u)C_{\mathcal{O}\mathcal{O}}(m-t) \\ &\quad + \kappa(t, m, m+u)] + o\left(\frac{1}{n}\right), \end{aligned} \quad (3.6)$$

where  $t, u \geq 0$  and  $\kappa$  is the connected 4-point autocorrelation function

$$\begin{aligned} \kappa(r, s, t) &\equiv \langle (\mathcal{O}_i - \mu_{\mathcal{O}})(\mathcal{O}_{i+r} - \mu_{\mathcal{O}})(\mathcal{O}_{i+s} - \mu_{\mathcal{O}})(\mathcal{O}_{i+t} - \mu_{\mathcal{O}}) \rangle \\ &\quad - C_{\mathcal{O}\mathcal{O}}(r)C_{\mathcal{O}\mathcal{O}}(t-s) - C_{\mathcal{O}\mathcal{O}}(s)C_{\mathcal{O}\mathcal{O}}(t-r) \\ &\quad - C_{\mathcal{O}\mathcal{O}}(t)C_{\mathcal{O}\mathcal{O}}(s-r). \end{aligned} \quad (3.7)$$

The natural estimator for the normalized autocorrelation function  $\rho_{\mathcal{O}\mathcal{O}}(t)$  is

$$\widehat{\rho}_{\mathcal{O}\mathcal{O}}(t) \equiv \frac{\widehat{C}_{\mathcal{O}\mathcal{O}}(t)}{\widehat{C}_{\mathcal{O}\mathcal{O}}(0)} \quad (3.8)$$

if the mean  $\mu_{\mathcal{O}}$  is known, and

$$\widehat{\widehat{\rho}}_{\mathcal{O}\mathcal{O}}(t) \equiv \frac{\widehat{\widehat{C}}_{\mathcal{O}\mathcal{O}}(t)}{\widehat{\widehat{C}}_{\mathcal{O}\mathcal{O}}(0)} \quad (3.9)$$

if the mean  $\mu_{\mathcal{O}}$  is unknown. The estimators  $\widehat{\rho}_{\mathcal{O}\mathcal{O}}(t)$  and  $\widehat{\widehat{\rho}}_{\mathcal{O}\mathcal{O}}(t)$  are biased by terms of order  $1/n$ , as a result of the ratios of random variables in (3.8)/(3.9). The covariance matrices of  $\widehat{\rho}_{\mathcal{O}\mathcal{O}}$  and  $\widehat{\widehat{\rho}}_{\mathcal{O}\mathcal{O}}$  are the same to leading order in  $1/n$ . If the process is Gaussian, this covariance matrix is given in the large- $n$  limit by [37]

$$\begin{aligned} \text{cov}(\widehat{\rho}_{\mathcal{O}\mathcal{O}}(t), \widehat{\rho}_{\mathcal{O}\mathcal{O}}(u)) &= \frac{1}{n} \sum_{m=-\infty}^{\infty} [\rho_{\mathcal{O}\mathcal{O}}(m)\rho_{\mathcal{O}\mathcal{O}}(m+t-u) + \rho_{\mathcal{O}\mathcal{O}}(m+u)\rho_{\mathcal{O}\mathcal{O}}(m-t) \\ &\quad + 2\rho_{\mathcal{O}\mathcal{O}}(t)\rho_{\mathcal{O}\mathcal{O}}(u)\rho_{\mathcal{O}\mathcal{O}}^2(m) - 2\rho_{\mathcal{O}\mathcal{O}}(t)\rho_{\mathcal{O}\mathcal{O}}(m)\rho_{\mathcal{O}\mathcal{O}}(m-u) \\ &\quad - 2\rho_{\mathcal{O}\mathcal{O}}(u)\rho_{\mathcal{O}\mathcal{O}}(m)\rho_{\mathcal{O}\mathcal{O}}(m-t)] + o\left(\frac{1}{n}\right) \end{aligned} \quad (3.10)$$

for  $t, u \geq 0$ . If the process is *not* Gaussian, then there are additional terms proportional to the fourth cumulant  $\kappa(m, t, t-u)$ . The simplest assumption is to consider the stochastic process to be “not too far from Gaussian”, and drop all the terms involving  $\kappa$ . If this assumption is *not* justified, then we are introducing a bias in the estimate of this covariance.

Finally, we shall take the estimator for the integrated autocorrelation time to be [38]

$$\widehat{\tau}_{\text{int},\mathcal{O}} \equiv \frac{1}{2} \sum_{t=-M}^M \widehat{\rho}_{\mathcal{O}\mathcal{O}}(t) \quad (3.11)$$

[or the same thing with  $\widehat{\rho}_{\mathcal{O}\mathcal{O}}(t)$ ] where  $M$  is a suitably chosen number. The reason behind the cutoff  $M$  is the following: if we were to make the “obvious” choice  $M = n + 1$ , then the resulting estimator would have a variance of order 1 even in the limit  $n \rightarrow \infty$ ; this is because the terms  $\widehat{\rho}_{\mathcal{O}\mathcal{O}}(t)$  with large  $t$  have errors (of order  $1/n$ ) that *do not* vanish as  $t$  grows [cf. (3.10)], and their number is also large ( $\sim n$ ). Taking  $M \ll n$  restores the good behavior of the estimator as  $n \rightarrow \infty$ . The bias introduced by this rectangular cutoff<sup>10</sup> is given by

$$\text{bias}(\widehat{\tau}_{\text{int},\mathcal{O}}) = -\frac{1}{2} \sum_{|t|>M} \rho_{\mathcal{O}\mathcal{O}}(t) + o\left(\frac{1}{n}\right). \quad (3.12)$$

The variance of the estimator  $\widehat{\tau}_{\text{int},\mathcal{O}}$  can be computed from the covariance (3.10); the final result is [38]

$$\text{var}(\widehat{\tau}_{\text{int},\mathcal{O}}) \approx \frac{2(2M+1)}{n} \tau_{\text{int},\mathcal{O}}^2, \quad (3.13)$$

where the approximation  $\tau_{\text{int},\mathcal{O}} \ll M \ll n$  has been made. A good (self-consistent) choice of  $M$  is the following [38]: let  $M$  be the smallest integer such that  $M \geq c\widehat{\tau}_{\text{int},\mathcal{O}}(M)$ , where  $c$  is a suitable constant. If the normalized autocorrelation function is roughly a pure exponential<sup>11</sup>, then a choice in the range  $c \approx 6$ – $8$  is reasonable. Indeed, if we take  $\rho_{\mathcal{O}\mathcal{O}}(t) = e^{-t/\tau}$  and minimize the mean-square error

$$\text{MSE}(\widehat{\tau}_{\text{int},\mathcal{O}}) \equiv \text{bias}(\widehat{\tau}_{\text{int},\mathcal{O}})^2 + \text{var}(\widehat{\tau}_{\text{int},\mathcal{O}}) \quad (3.14)$$

using (3.12)/(3.13), we find that the optimal window width is

$$M_{\text{opt}} = \frac{\tau}{2} \log\left(\frac{n}{2\tau}\right) - 1. \quad (3.15)$$

For  $n/\tau \approx 10^8$  (resp.  $10^6$ ,  $10^4$ ), we have  $M_{\text{opt}}/\tau \approx 8.86$  (resp. 6.56, 4.26). In this paper we used  $c = 8$  for the observables  $\mathcal{N}$ ,  $\mathcal{E}$ ,  $\mathcal{E}'$ ,  $\mathcal{M}^2$ ,  $\mathcal{S}_2$  and  $\mathcal{C}_1$ , whose autocorrelation functions are close to a pure exponential (see Section 5.2);  $c = 10$  for  $\mathcal{S}_0$ ; and  $c = 15$  for  $\mathcal{C}_2$  and  $\mathcal{C}_3$ .

As noted above, we expect the estimator  $\widehat{\tau}_{\text{int},\mathcal{O}}$  to have a bias of order  $\tau_{\text{int},\mathcal{O}}/n$ , due to the nonlinearities in (3.8)/(3.9).<sup>12</sup> To make this bias negligible we need long runs. It has been shown empirically that this procedure works fairly well when  $n \gtrsim 10^4 \widehat{\tau}_{\text{int},\mathcal{O}}$  [4].

**Remarks.** 1. For the specific heat  $C_H$  and the correlation length  $\xi$ , which are “composite” quantities (i.e. not merely the mean value of a single observable), the estimation of the error bars is a bit more complicated. One method is described in [11, Section 4]; a slightly better method, based on the analysis of the cross-correlation matrix, is described in [31].

---

<sup>10</sup>We could use more general cutoff functions, but this rectangular cutoff is the most convenient for the present purposes.

<sup>11</sup>This is confirmed here for the observables  $\mathcal{N}$ ,  $\mathcal{E}$ ,  $\mathcal{E}'$ ,  $\mathcal{M}^2$ ,  $\mathcal{S}_2$  and  $\mathcal{C}_1$  (see Section 5.2). Similar behavior is found in the SW algorithm for the two-dimensional Ising [10], 3-state Potts [11] and 4-state Potts models [12].

<sup>12</sup>The bias on the estimator  $\widehat{\tau}_{\text{int},\mathcal{O}}$  also induces a bias on the estimated variance (3.3) of the sample mean  $\overline{\mathcal{O}}$ . This bias is of order  $1/n^2$ , i.e. a factor  $1/n$  down from the variance (3.3) itself.

2. On most lattices we made a number of independent runs, rather than one long run (see Section 4 below). Our best estimate of each autocorrelation function  $\rho_{\mathcal{O}\mathcal{O}}(t)$  was then obtained by averaging the estimates  $\hat{\rho}_{\mathcal{O}\mathcal{O}}(t)$  from the individual runs, with weights proportional to the run lengths. Finally, the windowing procedure was performed on the resulting best estimate of  $\rho_{\mathcal{O}\mathcal{O}}(t)$ . This is a better procedure than performing the windowing on each run separately.

3. As a check on the correctness of the error bars produced by our time-series-analysis method, we also used an analysis method based on independent “bunches” [11, Section 4.2]. The error bars ranged from  $\approx 50\%$  to  $\approx 115\%$  of those produced by the time-series-analysis method, averaging around  $80\%$ . The fluctuations are not surprising, as the bunch-method error bar has a statistical fluctuation of order  $1/\sqrt{m}$ , where  $m$  is the number of bunches (in our case ranging from 10 to 35). However, the systematic tendency toward smaller error bars suggests that our time-series-analysis method may be slightly overestimating the error bars, probably due to neglect of the non-Gaussian terms in (3.10). Therefore, the true statistical error bars on our raw data and on our exponent estimates may be slightly smaller than those reported in this paper. This issue deserves a more detailed investigation in the future.

## 4 Description of the simulations

We implemented the Swendsen–Wang algorithm for the nearest-neighbor three-dimensional Ising model on an  $L \times L \times L$  simple-cubic lattice with periodic boundary conditions. We performed all our runs at  $\beta_{\text{Ising}} = 0.22165459$  (i.e.  $\beta_{\text{Potts}} = 0.44330918$ ), which is Blöte *et al.*’s [39] best estimate of the critical temperature and is very near to the estimates by other workers [40, 41] (see also the review [42]). We studied lattice sizes  $L = 4, 6, 8, 12, 16, 24, 32, 48, 64, 96, 128, 192, 256$  and performed between  $2.9 \times 10^7$  and  $5 \times 10^8$  SW iterations for each lattice size (see Table 1). The total data set at each  $L$  corresponds to  $\approx 10^6\tau$  on the largest lattices ( $L = 192, 256$ ), at least  $10^7\tau$  on all  $L \leq 64$ , and nearly  $10^8\tau$  at  $L = 16$  (see again Table 1). In all cases, the statistics are high enough to permit a high accuracy in our estimates of the static (error  $\sim 0.01\text{--}0.12\%$ ) and dynamic (error  $\sim 0.1\text{--}0.5\%$ ) quantities. Our results for the principal static observables are reported in Table 2, and for the dynamic quantities in Tables 3 and 4.

The initial configuration of each run was either random or ordered, and we discarded the first  $10^5$  iterations from each run in order to allow the system to reach equilibrium; this discard interval is in all cases greater than  $4000\tau_{\text{int},\mathcal{E}'}$ , which is more than sufficient.<sup>13</sup> We

---

<sup>13</sup>Such a discard interval might seem to be much larger than necessary:  $100\tau_{\text{exp}}$  would usually be more than enough. However, there is always the danger that the longest autocorrelation time in the system ( $\tau_{\text{exp}}$ ) may be much larger than the longest autocorrelation time that one has *measured*, because one has failed to measure an observable having sufficiently strong overlap with the slowest mode. As an undoubtedly overly conservative precaution against the possible (but unlikely) existence of such a (vastly) slower mode, we decided to discard  $10^5$  iterations. In most cases this amounts to less than 10% of the run, thus reducing the accuracy on our final estimates by less than 5%. Unless there exists a vastly slower mode of which we are unaware, our data yield  $\tau_{\text{int},\mathcal{E}'}/\tau_{\text{exp}} \approx 0.9\text{--}1$  for this algorithm (see Section 5.2 and Table 8 below). So the discard interval is greater than  $4000\tau_{\text{exp}}$ .

checked that random and ordered initial conditions gave identical results, within statistical error. On some of the smaller lattices, we made a single long run of  $10^8$  iterations; on other lattices, we averaged the data from several (anywhere from 2 to 46) individual runs of at least  $10^6$  iterations each (except for a small number of runs of length  $5 \times 10^5$  at  $L = 96, 192, 256$ ). In all cases we discarded the first  $10^5$  iterations of each run. The individual runs (minus the discard) are all of length greater than  $20000\tau_{\text{int},\mathcal{E}'}$ , which is long enough to allow a good determination of the dynamic quantities.

Our program was written in Fortran 77 and run on a 1266 MHz Pentium III Tualatin processor using the g77 Fortran compiler. Our program requires approximately  $42L^3$  bytes memory. The CPU time required by our program ranges from 0.39 to 0.90  $L^3 \mu\text{s}/\text{iteration}$ , depending on the lattice size (see Table 1). The sharp rise in CPU time per spin on very small lattices arises from the “fixed costs” of the algorithm (i.e. those that do not scale with the volume). The slow rise in CPU time per spin on larger lattices arises from the “cache misses” that occur, due to the nonlocal nature of the Swendsen–Wang algorithm, when the lattice no longer fits in the 512 KB cache. The total CPU time used in these runs was approximately 17.8 years.

In the first version of our program, the random numbers were supplied by a linear congruential generator

$$x_{n+1} = ax_n + c \pmod{m} \quad (4.1)$$

with modulus  $m = 2^{48}$ , increment  $c = 1$ , and multiplier  $a = 3116728, 10430376854301, 77596615844045$  or  $181465474592829$ . All these multipliers give good results on the spectral test in low dimensions, compared to other multipliers for the same modulus [43, 44]. We verified that the runs with the four different multipliers gave results that are consistent within error bars for all the major observables. But when we analyzed the data for  $\xi/L$ , which ought to behave according to the finite-size scaling Ansatz

$$\xi/L = x^* + AL^{-\omega} + \dots \quad (4.2)$$

where  $x^*$  is a universal amplitude ratio and  $\omega$  is a correction-to-scaling exponent, we found that our data fit this Ansatz very well (with  $\omega = 0.82$  from [39]) *except for the points at  $L = 128$  and  $L = 256$* , which showed deviations of magnitude 3% ( $\approx 79$  standard deviations) and 21% ( $\approx 170$  standard deviations), respectively. Clearly something was going very wrong!

After much work, we traced these systematic errors to the effects of long-range correlations (at lags that are multiples of large powers of 2) in the random-number generator [45–48]. It turns out [48] that these long-range correlations can arise within a single bond-update half-sweep of the Swendsen–Wang algorithm, provided that the lattice size is large enough compared to the modulus of the random-number generator. In a separate paper [48] we have studied these systematic errors in detail, in an effort to determine their approximate magnitude as a function of the lattice size and the random-number-generator modulus. Suffice it to say here that the systematic errors with a 48-bit random-number generator are comparable to or larger than our statistical errors *only* when the lattice size is a multiple of 64, which in this paper means  $L = 64, 128, 192, 256$ . We therefore *discarded* all the data for these lattices ( $\approx 9.5$  years CPU time, alas!) and performed new runs using 60-bit, 63-bit and 64-bit random-number generators:



Modulus  $m = 2^{60}$ , multiplier  $a = 454339144066433781$ .

Modulus  $m = 2^{63}$ , multiplier  $a = 9219741426499971445$ .

Modulus  $m = 2^{64}$ , multiplier  $a = 3202034522624059733$ .

(All these multipliers give good results on the spectral test in low dimensions, compared to other multipliers for the same modulus [43, 44].) We also performed some additional runs on the smaller lattices using these generators. We have convinced ourselves [48] that generators using  $\geq 60$  bits will exhibit significant systematic errors *only* on lattices larger than  $L = 256$ ; in addition, they *may* exhibit slight systematic errors, less than about  $2\sigma$ , also at  $L = 256$  (we are currently investigating this latter issue more carefully).

We assure the reader that the data reported in the present paper include *only* runs using “safe” random-number generators, i.e.  $m \geq 2^{60}$  for  $L = 64, 128, 192, 256$ , and  $m \geq 2^{48}$  for all other  $L$ . The CPU time figure of 17.8 years refers to these “good” runs only.

## 5 Data analysis

For each quantity  $\mathcal{O}$ , we carry out a fit to the power-law Ansatz  $\mathcal{O} = AL^p$  using the standard weighted least-squares method. As a precaution against corrections to scaling, we impose a lower cutoff  $L \geq L_{\min}$  on the data points admitted in the fit, and we study systematically the effects of varying  $L_{\min}$  on the estimates of  $A$  and  $p$  and on the  $\chi^2$  value. In general, our preferred fit corresponds to the smallest  $L_{\min}$  for which the goodness of fit is reasonable (e.g., the confidence level<sup>14</sup> is  $\gtrsim 10$ –20%), and for which subsequent increases in  $L_{\min}$  do not cause the  $\chi^2$  to drop vastly more than one unit per degree of freedom.

The behavior of the static quantities will be discussed in a separate paper [31]. Here we limit attention to the dynamic quantities.

### 5.1 Integrated autocorrelation times

Let us begin by summarizing the qualitative behavior of the integrated autocorrelation times  $\tau_{\text{int},\mathcal{O}}$  for different observables  $\mathcal{O}$ , as reported in Tables 3 and 4. The three “energy-like” observables  $\mathcal{N}, \mathcal{E}, \mathcal{E}'$  satisfy

$$\tau_{\text{int},\mathcal{N}} \leq \tau_{\text{int},\mathcal{E}} \leq \tau_{\text{int},\mathcal{E}'} \quad (5.1)$$

and the two “susceptibility-like” observables  $\mathcal{M}^2, \mathcal{S}_2$  satisfy

$$\tau_{\text{int},\mathcal{M}^2} \leq \tau_{\text{int},\mathcal{S}_2} \quad (5.2)$$

in accordance with a rigorous theorem [11, 25]. These five observables all have autocorrelation times in the same ballpark, as do  $\mathcal{C}_1$  and  $\mathcal{S}_0$ . The autocorrelation times of  $\mathcal{C}_2$  and  $\mathcal{C}_3$ , by

---

<sup>14</sup>“Confidence level” is the probability that  $\chi^2$  would exceed the observed value, assuming that the underlying statistical model is correct. An unusually low confidence level (e.g., less than 5%) thus suggests that the underlying statistical model is *incorrect* — the most likely cause of which would be corrections to scaling not included in the Ansatz.

contrast, are notably smaller. Of all the observables we measured,  $\mathcal{E}'$  exhibits the largest autocorrelation time, with  $\mathcal{E}$  and  $\mathcal{S}_2$  only slightly behind.

Let us now fit the integrated autocorrelation times for all these observables to a simple power law  $\tau_{\text{int},\mathcal{O}} = AL^{z_{\text{int},\mathcal{O}}}$ . We shall show the case of  $\mathcal{E}'$  in detail; all the other observables behave similarly.

In Figure 1 we have made a log-log plot of  $\tau_{\text{int},\mathcal{E}'}$  versus  $L$ . (Please note that the error bars are significantly smaller than the plot symbols.) The plot shows notable curvature, i.e. there are fairly strong corrections to scaling, at least for  $L \lesssim 64$ . Consequently, the least-squares fits with  $L_{\min} \leq 64$  all have enormous  $\chi^2$  (confidence level  $< 0.05\%$ ), reflecting the fact that for  $L \lesssim 64$  the corrections to scaling are many times our (very small) error bars. For  $L_{\min} \geq 96$ , by contrast, the  $\chi^2$  values are good, reflecting the fact that in this regime the corrections to scaling are comparable to or smaller than our error bars. Our preferred fit corresponds to  $L_{\min} = 96$ , and yields

$$z_{\text{int},\mathcal{E}'} = 0.4588 \pm 0.0047 \quad (5.3)$$

with  $\chi^2 = 0.352$  (2 DF, level = 83.8%); here the error bar is one standard deviation (i.e. confidence level  $\approx 68\%$ ).

A similar pattern is obtained for all the other observables, with the curvature always in the same direction. In all cases our preferred fit corresponds to  $L_{\min} = 96$ ; the results of these fits are reported in Table 5. All the observables except  $\mathcal{C}_2$  and  $\mathcal{C}_3$  have exponents  $z_{\text{int}}$  in the vicinity  $0.45 \pm 0.03$ . It is conceivable that the true values of these exponents are in fact *exactly* equal; we do not know whether the small differences between the estimates represent real differences or are merely the residual effects of corrections to scaling.

It is worth noting that the rigorous inequality (5.1) implies

$$z_{\text{int},\mathcal{N}} \leq z_{\text{int},\mathcal{E}} \leq z_{\text{int},\mathcal{E}'} , \quad (5.4)$$

while the estimates in Table 5 show the *opposite* behavior. This strongly suggests that in fact we have

$$z_{\text{int},\mathcal{N}} = z_{\text{int},\mathcal{E}} = z_{\text{int},\mathcal{E}'} , \quad (5.5)$$

in accordance with the “almost-theorem” proven in [11, Section 2.2], and that the deviations in Table 5 result from corrections to scaling. Unfortunately, we don’t know which of these estimates is closest to the true value; but we are inclined to trust more the estimate coming from the slowest of these modes, i.e.  $\mathcal{E}'$ . We therefore give as our final estimate

$$z_{\text{int},\mathcal{N}} = z_{\text{int},\mathcal{E}} = z_{\text{int},\mathcal{E}'} = 0.459 \pm 0.005 \pm 0.025 , \quad (5.6)$$

where the first error bar represents statistical error (68% confidence interval) and the second error bar represents possible systematic error due to the residual effects of corrections to scaling (68% subjective confidence interval).

The susceptibility-like observables  $\mathcal{M}^2$  and  $\mathcal{S}_2$ , by contrast, do show the correct inequality arising from (5.2). Comparing the two estimated exponents, and bearing in mind the “almost-theorem” that they should be equal, we give as our final estimate

$$z_{\text{int},\mathcal{M}^2} = z_{\text{int},\mathcal{S}_2} = 0.443 \pm 0.005 \pm 0.030 . \quad (5.7)$$

The estimates (5.6) and (5.7) are consistent with each other, as well as with the estimates for  $z_{\text{int},\mathcal{S}_0}$  and  $z_{\text{int},\mathcal{C}_1}$ . This suggests that the true values of all these exponents might be exactly equal. Only the estimates for  $z_{\text{int},\mathcal{C}_2}$  and  $z_{\text{int},\mathcal{C}_3}$  are significantly lower than the others; and even here, it is conceivable that the discrepancy again arises from corrections to scaling.

## 5.2 Exponential autocorrelation time and autocorrelation functions

Recall that exponential autocorrelation time of an observable  $\mathcal{O}$  is defined as

$$\tau_{\text{exp},\mathcal{O}} = \lim_{t \rightarrow \infty} \frac{-|t|}{\log \rho_{\mathcal{O}\mathcal{O}}(t)} , \quad (5.8)$$

and that the exponential autocorrelation time of the system is defined as

$$\tau_{\text{exp}} = \sup_{\mathcal{O}} \tau_{\text{exp},\mathcal{O}} . \quad (5.9)$$

All observables that are not orthogonal to the system's slowest mode satisfy  $\tau_{\text{exp},\mathcal{O}} = \tau_{\text{exp}}$ . Since all the observables studied in this paper are invariant under the symmetry group of the Potts model, we have no reason to expect that any of them are orthogonal to the slowest mode. We therefore expect — and will verify numerically — that they all have the *same* exponential autocorrelation time  $\tau_{\text{exp},\mathcal{O}}$ , which is presumably equal to  $\tau_{\text{exp}}$ .

We shall begin by discussing the qualitative behavior of the autocorrelation functions for various observables at fixed  $L$ . Then we shall discuss the  $L$ -dependence of various quantities associated to the exponential decay of the autocorrelation functions. Finally, in the next subsection, we shall discuss the finite-size scaling of the autocorrelation functions.

The typical behavior of the autocorrelation functions  $\rho_{\mathcal{O}\mathcal{O}}(t)$  is depicted in Figure 2. For simplicity we have shown only the two observables exhibiting the most extreme behavior (among these we have measured): namely,  $\mathcal{E}'$ , which has the largest  $\tau_{\text{int}}$  and whose autocorrelation function shows the least curvature (i.e. is closest to a pure exponential); and  $\mathcal{C}_2$ , which has the smallest  $\tau_{\text{int}}$  and whose autocorrelation function shows the most curvature. The plots for all other observables are intermediate between these two.<sup>15</sup> Clearly, each autocorrelation function behaves asymptotically for large  $t$  as

$$\rho_{\mathcal{O}\mathcal{O}}(t) \approx A_{\mathcal{O}} e^{-|t|/\tau_{\text{exp},\mathcal{O}}} . \quad (5.10)$$

We obtained rough estimates of  $\tau_{\text{exp},\mathcal{O}}$  and the amplitude  $A_{\mathcal{O}}$  by performing an unweighted least-squares fit to

$$\log \rho_{\mathcal{O}\mathcal{O}}(t) = a - bt \quad (5.11)$$

---

<sup>15</sup>These behaviors underlie our choice of the window factors for estimating  $\tau_{\text{int},\mathcal{O}}$ : namely,  $c = 8$  for  $\mathcal{N}$ ,  $\mathcal{E}$ ,  $\mathcal{E}'$ ,  $\mathcal{M}^2$ ,  $\mathcal{S}_2$  and  $\mathcal{C}_1$ , whose autocorrelation functions are close to a pure exponential;  $c = 10$  for  $\mathcal{S}_0$ ; and  $c = 15$  for  $\mathcal{C}_2$  and  $\mathcal{C}_3$ .

over the range  $\tau_{\text{int},\mathcal{E}'} \leq t \leq 3\tau_{\text{int},\mathcal{E}'}$  where all the autocorrelation functions are approximately a pure exponential; this yields  $\tau_{\text{exp},\mathcal{O}} = 1/b$  and  $A_{\mathcal{O}} = e^a$ .<sup>16</sup> The results are shown in Tables 6 and 7. Clearly, all the observables studied here have the same value of  $\tau_{\text{exp},\mathcal{O}}$ , as expected theoretically. We shall use  $\tau_{\text{exp},\mathcal{E}'}$  from Table 6 as our best estimate of  $\tau_{\text{exp}}$ .

In Figure 3 we have plotted the estimated  $\tau_{\text{exp}}$  versus  $L$ . We attempted to estimate the dynamic critical exponent  $z_{\text{exp}}$  by fitting

$$\tau_{\text{exp}} \approx BL^{z_{\text{exp}}} . \quad (5.12)$$

In performing this fit, we used as rough error bars on  $\tau_{\text{exp}}$  the sum of the error bar on  $\tau_{\text{int},\mathcal{E}'}$  and the standard deviation of the  $\tau_{\text{exp}}$  estimates for the seven observables  $\mathcal{N}$ ,  $\mathcal{E}$ ,  $\mathcal{E}'$ ,  $\mathcal{M}^2$ ,  $\mathcal{S}_2$ ,  $\mathcal{S}_0$  and  $\mathcal{C}_1$ . Our preferred fit has  $L_{\text{min}} = 96$ , and yields  $z_{\text{exp}} = 0.481 \pm 0.007$ ,  $B = 1.706 \pm 0.058$  ( $\chi^2 = 0.754$ , 2 DF, level = 68.6%). Of course, these error bars should not be taken terribly seriously.

It is not clear whether  $z_{\text{exp}}$  is equal to  $z_{\text{int},\mathcal{E}'}$  or is slightly larger. This question is related to the degree of curvature in the plot of the autocorrelation function, and more specifically to its  $L$ -dependence. To investigate this question in more detail, we first observed that

$$A_{\mathcal{O}} e^{-|t|/\tau_{\text{exp}}} \leq \rho_{\mathcal{O}\mathcal{O}}(t) \leq e^{-|t|/\tau_{\text{exp}}} \quad (5.13)$$

(as is obvious from Figure 2). Therefore, if we define the modified autocorrelation time

$$\bar{\tau}_{\text{exp}} \equiv \frac{1}{2} \sum_{t=-\infty}^{\infty} e^{-|t|/\tau_{\text{exp}}} = \frac{1}{2} \frac{1 + e^{-1/\tau_{\text{exp}}}}{1 - e^{-1/\tau_{\text{exp}}}} , \quad (5.14)$$

we necessarily have

$$A_{\mathcal{O}} \leq \frac{\tau_{\text{int},\mathcal{O}}}{\bar{\tau}_{\text{exp}}} \leq 1 . \quad (5.15)$$

We therefore studied the  $L$ -dependence of the quantities  $A_{\mathcal{O}}$  and  $R_{\mathcal{O}} \equiv \tau_{\text{int},\mathcal{O}}/\bar{\tau}_{\text{exp}}$  for various observables  $\mathcal{O}$  (see Tables 8 and 9).

We tried fits of  $A_{\mathcal{O}}$  and  $R_{\mathcal{O}}$  to the alternative Ansätze  $cL^{-p}$  and  $c_1 + c_2 L^{-\omega}$  (with  $\omega = 0.82$ ). Unfortunately, we do not have any valid error bars on  $A_{\mathcal{O}}$  and  $R_{\mathcal{O}}$ ; but we can assign fictitious error bars and compare the *relative*  $\chi^2$  for the two fits. We did this for the two extreme observables,  $\mathcal{E}'$  and  $\mathcal{C}_2$ . In all cases we found that the power-law Ansatz gives a much better fit, and also one that holds over a wider range of  $L$ . We estimated  $p \approx 0.023$  for  $A_{\mathcal{E}'}$ ,  $p \approx 0.021$  for  $R_{\mathcal{E}'}$ ,  $p \approx 0.092$  for  $A_{\mathcal{C}_2}$ ,  $p \approx 0.135$  for  $R_{\mathcal{C}_2}$ . The values for  $p$  for  $A_{\mathcal{E}'}$  and  $R_{\mathcal{E}'}$  are very nearly equal, and are almost exactly equal to our estimate of  $z_{\text{exp}} - z_{\text{int},\mathcal{E}'} \approx 0.022$ . As for the values for  $p$  for  $A_{\mathcal{C}_2}$  and  $R_{\mathcal{C}_2}$ , they violate the rigorous inequality  $p(A_{\mathcal{C}_2}) \geq p(R_{\mathcal{C}_2})$  that follows from (5.15); this strongly suggests that the two exponents  $p(A_{\mathcal{C}_2})$  and  $p(R_{\mathcal{C}_2})$  are in fact equal, though we do not know whether the correct value lies nearer to 0.092 or to 0.135. The latter value is fairly close to our estimate of  $z_{\text{exp}} - z_{\text{int},\mathcal{C}_2} \approx 0.127$ .

---

<sup>16</sup>In principle we should have done a properly weighted least-squares fit, taking account of the covariance matrix (3.10) among the estimates  $\hat{\rho}_{\mathcal{O}\mathcal{O}}(t)$ . But this is rather complicated, and we did not think it was worth the effort. As a result of this laziness, we are unable to quote any reliable error bars on  $\tau_{\text{exp},\mathcal{O}}$  or  $A$ .

Since for each of these observables it appears that  $A_{\mathcal{O}}$  and  $R_{\mathcal{O}}$  have the same exponent  $p$ , we tried fits of  $R_{\mathcal{O}}/A_{\mathcal{O}}$  to the Ansatz  $c_1 + c_2 L^{-\omega}$  (with  $\omega = 0.82$ ). For  $\mathcal{E}'$  we find a limiting value  $R_{\mathcal{E}'}/A_{\mathcal{E}'} \approx 1.010$ ; for  $\mathcal{C}_2$  it is more difficult to tell, but a limiting value  $R_{\mathcal{C}_2}/A_{\mathcal{C}_2} \approx 1.14$  seems plausible.

### 5.3 Finite-size scaling of autocorrelation functions

A final way to study these questions is to investigate the finite-size scaling of the autocorrelation functions. The standard dynamic finite-size-scaling Ansatz for the autocorrelation function  $\rho_{\mathcal{O}\mathcal{O}}(t)$  is

$$\rho_{\mathcal{O}\mathcal{O}}(t; L) \approx |t|^{-p_{\mathcal{O}}} h_{\mathcal{O}}\left(\frac{t}{\tau_{\text{exp},\mathcal{O}}}; \frac{\xi(L)}{L}\right). \quad (5.16)$$

(Here the dependence on the coupling constants, e.g. the inverse temperature, has been suppressed for notational simplicity.) Summing (5.16) over  $t$ , it follows that

$$\tau_{\text{int},\mathcal{O}} \sim \tau_{\text{exp},\mathcal{O}}^{1-p_{\mathcal{O}}}, \quad (5.17)$$

or equivalently,

$$z_{\text{int},\mathcal{O}} = (1 - p_{\mathcal{O}}) z_{\text{exp},\mathcal{O}}. \quad (5.18)$$

Thus, only when  $p_{\mathcal{O}} = 0$  do we have  $z_{\text{int},\mathcal{O}} = z_{\text{exp},\mathcal{O}}$  [4]. In this latter case the Ansatz (5.16) can be rewritten in the equivalent form

$$\rho_{\mathcal{O}\mathcal{O}}(t; L) \approx \hat{h}_{\mathcal{O}}\left(\frac{t}{\tau_{\text{int},\mathcal{O}}}; \frac{\xi(L)}{L}\right). \quad (5.19)$$

To test this latter Ansatz, we have plotted  $\log \rho_{\mathcal{O}\mathcal{O}}(t)$  versus  $t/\tau_{\text{int},\mathcal{O}}$  for the observable  $\mathcal{O} = \mathcal{E}'$  (Figure 4). For clarity we have included only the data from  $L \geq 12$ ; the data coming from different lattice sizes are plotted with different symbols. We have also depicted for reference a line corresponding to the pure exponential  $\rho_{\mathcal{E}'\mathcal{E}'}(t) = e^{-t/\tau_{\text{int},\mathcal{E}'}}$ .

The data fall roughly onto a single curve, but there are clear corrections to scaling: the points move upwards (away from the pure exponential line) as  $L$  increases. It is not clear whether the points are tending to a limiting curve as  $L \rightarrow \infty$ , or whether they will continue indefinitely to move upwards. This is another way of saying that we do not know whether  $p_{\mathcal{E}'} = 1 - z_{\text{int},\mathcal{E}'}/z_{\text{exp}}$  is exactly zero or is slightly positive (e.g.  $\approx 0.067$ ).

## 6 Discussion

In this paper we have obtained high-precision data at the critical point of the three-dimensional Ising model on fairly large lattices (up to  $L = 256$ ), which have allowed us to derive quite accurate estimates of the dynamic critical exponents  $z_{\text{int},\mathcal{O}}$  and  $z_{\text{exp}}$  for the Swendsen–Wang algorithm for this model. Our data resolve the discrepancies between previous works [9, 14–20], which can now be understood as arising from corrections to scaling.

We would like to conclude by comparing our numerical results with some of the theoretical frameworks that have been proposed by previous authors. These frameworks have

as their goal to understand the dynamic critical behavior of the Swendsen–Wang algorithm for the various ferromagnetic Potts models, and in particular to relate the dynamic critical exponent(s)  $z_{\text{SW}}$  to the *static* critical exponents for the same models. The three most important of these frameworks are the Li–Sokal proof [25] and its extensions [11, 12]; the scaling Ansatz of Klein, Ray and Tamayo [21]; and the empirically based conjectures of Coddington and Baillie [16].

We have discussed the Li–Sokal bound  $z_{\text{SW}} \geq \alpha/\nu$  in the Introduction, and there is not much more to say. Suffice it to observe once again that while this bound is close to sharp (and possibly even sharp modulo a logarithm) for the two-dimensional Potts models with  $q = 2, 3, 4$ , it is clearly far from sharp in the three- and four-dimensional Ising models. Our data for the three-dimensional Ising model yield  $z_{\text{SW}} \approx 0.46$ , compared to  $\alpha/\nu \approx 0.1756$  [41]; and for the four-dimensional Ising model it is generally believed that  $z_{\text{SW}} = 1$  [16, 21–24], compared to  $\alpha/\nu = 0$  ( $\times \log^{1/3}$ ). Clearly, some other physical mechanism, beyond the one exploited in the Li–Sokal proof, must be principally responsible for the critical slowing-down in these latter models; the central open problem is to identify this mechanism and to determine theoretically the dynamic critical exponent.

Klein, Ray and Tamayo [21] have presented a scaling Ansatz leading to the conjecture

$$z_{\text{SW}} = z_{\text{G}} - \frac{2\gamma}{d_m\nu}, \quad (6.1)$$

where  $z_{\text{G}}$  is the dynamic critical exponent for the Glauber dynamics in the same model, and  $d_m$  is “the mean fractal dimension of the finite clusters” in the Fortuin–Kasteleyn representation of the model.<sup>17</sup> The trouble with this Ansatz, alas, is not simply that the numerical value of  $d_m$  is unknown; it is, rather, that the definition of  $d_m$  is too vague to serve even as a guide for numerical attempts to determine its value. (The situation would be different if, for example,  $d_m$  could be defined as a dimension associated with the scaling behavior of some specific observable.) Consequently, Klein, Ray and Tamayo were limited in practice to observing that  $d_m$  presumably “lies between  $d$ , the spatial dimension, and  $d_f = d - \beta/\nu$ , the fractal dimension of the incipient infinite cluster” [21, p. 164]. This plausible reasoning yields the conjectured *inequality*

$$z_{\text{G}} - \frac{2\gamma}{d\nu - \beta} \leq z_{\text{SW}} \leq z_{\text{G}} - \frac{2\gamma}{d\nu}. \quad (6.2)$$

In Table 10 we compare  $z_{\text{SW}}$  with the Klein–Ray–Tamayo bounds  $z_{\text{KRT}}^{(\text{lower})}$  and  $z_{\text{KRT}}^{(\text{upper})}$  for the ferromagnetic Potts models (in dimension  $d \leq 4$ ) having a second-order transition. The bounds appear to be violated for all three two-dimensional Potts models: for the Ising and 3-state models, the violation is possibly within the errors in the determination of  $z_{\text{SW}}$  and  $z_{\text{G}}$ , especially if one takes into account the possibility of logarithms; but for the 4-state model, the violation is blatant (barring a gross error in the determination of  $z_{\text{G}}$ ). For the three-dimensional Ising model, curiously, the lower bound seems to be exact (within errors);

---

<sup>17</sup>The discussion of Klein, Ray and Tamayo [21] does not distinguish between the various dynamic critical exponents  $z_{\text{int},\text{O}}$  and  $z_{\text{exp}}$ . For simplicity we can assume that their discussion refers to  $z_{\text{exp}}$  for both the Swendsen–Wang and Glauber algorithms.

while for the four-dimensional Ising model, the upper bound is exact (modulo logarithms). It would be interesting to know whether the latter facts are anything more than curious coincidences.

Coddington and Baillie [16] carried out a careful numerical study of the dynamic critical behavior of the Swendsen–Wang algorithm for the Ising models in dimensions  $d = 2, 3, 4$ , on the basis of which they made the remarkable conjecture that for these models  $z_{\text{SW}} = \beta/\nu$  *exactly*. More specifically, they observed that the mean size of the largest cluster, here denoted  $C_1$ , scales at the critical point as  $C_1 \sim L^{d-\beta/\nu}$ , and they found that their data could be explained by the asymptotic Ansatz

$$\tau_{\text{SW}} C_1 / L^d \approx a + b \log L. \quad (6.3)$$

If true, this would imply that the correct dynamic critical exponent  $z_{\text{SW}}$  for the two-dimensional Ising model is neither 0 (log) [64] nor  $0.222 \pm 0.007$  [10], but rather  $1/8$  (possibly multiplied by a logarithm). The data of [10] are certainly consistent with this possibility, though they do not distinguish it from the other possible behaviors.<sup>18</sup>

For the three-dimensional Ising model, the Coddington–Baillie conjecture would imply that  $z_{\text{SW}} = 0.5183(4)$ , which at first sight is incompatible at the  $3\sigma$  level with our estimate  $z_{\text{int},\mathcal{E}'} = 0.459 \pm 0.005 \pm 0.025$  (central value  $\pm$  statistical error  $\pm$  systematic error). Indeed, the curvature in Figure 1, assuming that it continues in the same direction, suggests that the true  $z_{\text{int},\mathcal{E}'}$  is, if anything, slightly *lower* than our estimate based on  $L \leq 256$ . On the other hand, the difference between these exponents is small, and a small exponent is very difficult to distinguish from zero. We therefore made a direct test of the Coddington–Baillie conjecture by studying the combination  $\tau_{\text{int},\mathcal{E}'} C_1 / L^d$ . (Since we don’t have statistically valid error bars for this combination, we used the triangle inequality to set worst-case error bars.) A fit to  $\tau_{\text{int},\mathcal{E}'} C_1 / L^d = AL^p$  yields a decent  $\chi^2$  only for  $L_{\min} \geq 96$ ; our preferred fit is  $L_{\min} = 96$  and yields  $p = -0.0573 \pm 0.0052$ ,  $\log A = 0.670 \pm 0.025$  ( $\chi^2 = 0.261$ , 2 DF, level = 87.8%). This estimate for  $p$  is, not surprisingly, in almost perfect agreement with the values  $z_{\text{SW}} = 0.459$  and  $\beta/\nu = 0.5183$ .<sup>19</sup> On the other hand, if we fit to  $\tau_{\text{int},\mathcal{E}'} C_1 / L^d = A + BL^{-\omega}$  with  $\omega = 0.82$ , a decent  $\chi^2$  is again obtained only for  $L_{\min} \geq 96$ ; our preferred fit is again  $L_{\min} = 96$  and we get  $A = 1.362 \pm 0.011$ ,  $B = 6.064 \pm 0.553$  ( $\chi^2 = 1.726$ , 2 DF, level = 42.2%). Figure 5 shows the data points ( $\square$ ) and the corresponding fit. The fact that a reasonable fit is obtained with  $A$  far from zero (on the scale set by the observed values of  $\tau_{\text{int},\mathcal{E}'} C_1 / L^d$ ) means that our data are also consistent with a behavior  $\tau_{\text{int},\mathcal{E}'} C_1 / L^d \rightarrow A > 0$  as  $L \rightarrow \infty$ , and hence  $p = 0$ .

It is very hard (if not impossible) to distinguish, on purely numerical grounds, between these two behaviors. The  $\chi^2$  is slightly better for the power-law fit, but this minor difference should not be taken terribly seriously. The bottom line, it seems to us, is this: the data shown in Figure 5 do not give any strong reason to believe that  $\tau_{\text{int},\mathcal{E}'} C_1 / L^d$  is tending to *zero* as  $L \rightarrow \infty$ . Indeed, inspection of the curve would suggest a limit in the range 1.2–1.3,

---

<sup>18</sup>Unfortunately,  $C_1$  was not measured in [10].

<sup>19</sup>Just to be safe, we also checked the theoretically predicted scaling of  $C_1$ . Using the Ansatz  $C_1 / L^d = AL^p$ , we get a good fit already with  $L_{\min} = 48$ :  $p = -0.5162 \pm 0.0002$ ,  $\log A = 0.0892 \pm 0.0008$  ( $\chi^2 = 5.848$ , 4 DF, level = 21.1%). This value is not, strictly speaking, consistent with the estimate  $\beta/\nu = 0.5183(4)$ , but it is very close; the difference 0.002 can surely be understood as an effect of the residual corrections to scaling.

depending on the extent to which the curvature continues at larger  $L$ ; this predicted limit is only about 20% below the maximum value attained at  $L \approx 40$ , and is thus very far from zero. A more reliable judgment on the limiting value of  $\tau_{\text{int},\mathcal{E}}C_1/L^d$  will have to wait 5–10 years, when data will hopefully be available at (say)  $L = 512$  and  $L = 1024$ . But as things stand today, our data are fully consistent with the Coddington–Baillie conjecture (albeit without a logarithmic term).

If the Coddington–Baillie conjecture is interpreted as applying to  $z_{\text{exp}}$  rather than to  $z_{\text{int},\mathcal{E}'}$ , then the consistency between our data and the conjecture is even stronger. This is to be expected, as our estimate  $z_{\text{exp}} \approx 0.481$  is closer to the value  $\beta/\nu \approx 0.5183$ . The data points for  $\tau_{\text{exp},\mathcal{E}'}C_1/L^d$  are also shown (alas, without error bars) in Figure 5 (points \*). The curvature is slightly weaker than for  $\tau_{\text{int},\mathcal{E}'}C_1/L^d$ , and the data seem to be tending to a limit in the range 1.35–1.45.

Of course, as Coddington and Baillie [16] themselves observe,  $z_{\text{SW}} = \beta/\nu$  cannot possibly be a general identity for the Swendsen–Wang dynamics, as it clearly fails for the 2-dimensional Potts models with  $q = 3$  and  $q = 4$  (see Table 10). Indeed, the Li–Sokal bound (1.2) ensures that we must have  $z_{\text{SW}} > \beta/\nu$  in any Potts model where  $\alpha/\nu > \beta/\nu$ . At best, the identity  $z_{\text{SW}} = \beta/\nu$  could hold for the special case of the Ising models.

Since the Swendsen–Wang algorithm is defined naturally for all ferromagnetic Potts models, a theoretical framework that is valid only for the Ising case seems unnatural and, in our opinion, unlikely to be correct. But the Coddington–Baillie conjecture can be rephrased in the following way so as to be potentially valid for all Potts ferromagnets. Suppose that there exists an as-yet-not-understood physical mechanism causing slowness of the Swendsen–Wang dynamics that is somehow related to the typical size of the largest cluster. In this case, an inequality of the form

$$\tau_{\text{SW}} \geq \text{const} \times \frac{L^d}{C_1}, \quad (6.4)$$

analogous to the Li–Sokal bound (1.1), might hold for all Potts ferromagnets, irrespective of dimension and number of states. Indeed, it might even be possible to prove such an inequality rigorously (for one or another of the various autocorrelation times), if the physical basis were sufficiently well understood. Furthermore, it is even conceivable that the Li–Sokal mechanism and this new mechanism might together *exhaust* the reasons for slowness in the Swendsen–Wang dynamics, leading to the exact relation

$$z_{\text{SW}} = \max(\alpha/\nu, \beta/\nu) \quad (6.5)$$

(possibly modulo a logarithm) for all Potts ferromagnets. All currently available numerical data are consistent with the validity of the grand conjecture (6.5), provided that a multiplicative logarithm is permitted but not mandatory.

This conjecture is, of course, a wild speculation; indeed, we consider it unlikely, *a priori*, for a dynamic critical exponent of any nontrivial dynamics to be exactly expressible in terms of static critical exponents (except for trivial cases such as Gaussian models). But stranger things have happened; and this conjecture is, in any case, certainly worth closer investigation. More modestly, this line of reasoning suggests that efforts be made to prove the inequality (6.4) and to understand what kind of physical mechanism might cause it to hold.



## Acknowledgments

We wish to thank Henk Blöte, Lu s Antonio Fern ndez, Werner Kerler, Lev Shchur and Jian-Sheng Wang for valuable correspondence and for sharing their unpublished data; Mulin Ding and Raj Sivanandarajah for efficient assistance with numerous aspects of the Physics Department computing system; and Rom n Scoccimarro for generously letting us do some test runs on his DEC Alpha computer.

This research was supported in part by U.S. National Science Foundation grants PHY-0099393 and PHY-0116590.

## References

- [1] K.Binder, ed., *Monte Carlo Methods in Statistical Physics* (Springer-Verlag, Berlin, 1979, 2nd ed. 1986).
- [2] K. Binder, ed., *Applications of the Monte Carlo Method in Statistical Physics* (Springer-Verlag, Berlin, 1984, 2nd ed. 1987).
- [3] K. Binder, ed., *The Monte Carlo Method in Condensed Matter Physics* (Springer-Verlag, Berlin, 1992, 2nd ed. 1995).
- [4] A.D. Sokal, Monte Carlo methods in statistical mechanics: Foundations and new algorithms, in C. DeWitt-Morette, P. Cartier and A. Folacci, eds., *Functional Integration: Basics and Applications* (1996 Carg se summer school), pp. 131–192 (Plenum, New York, 1997).
- [5] M.E.J. Newman and G.T. Barkema, *Monte Carlo Methods in Statistical Physics* (Clarendon Press, Oxford–New York, 1999).
- [6] D.P. Landau and K. Binder, *A Guide to Monte Carlo Simulations in Statistical Physics* (Cambridge University Press, Cambridge–New York, 2000).
- [7] K. Binder and D.W. Heermann, *Monte Carlo Simulation in Statistical Physics: An Introduction*, 4th ed. (Springer-Verlag, Berlin–New York, 2002).
- [8] W. Janke, Math. Comput. Simulation **47**, 329 (1998).
- [9] R.H. Swendsen and J.-S. Wang, Phys. Rev. Lett. **58**, 86 (1987).
- [10] J. Salas and A.D. Sokal, Universal amplitude ratios in the critical two-dimensional Ising model on a torus, cond-mat/9904038v1, see Section 6. For space reasons, this material was deleted from the published version of this paper [J. Stat. Phys. **98**, 551 (2000)].
- [11] J. Salas and A.D. Sokal, J. Stat. Phys. **87**, 1 (1997), hep-lat/9605018.
- [12] J. Salas and A.D. Sokal, J. Stat. Phys. **85**, 297 (1996), hep-lat/9511022.

- [13] J. Salas and A.D. Sokal, J. Stat. Phys. **88**, 567 (1997), hep-lat/9607030.
- [14] U. Wolff, Phys. Lett. B **228**, 379 (1989).
- [15] J.-S. Wang, Physica A **164**, 240 (1990).
- [16] P.D. Coddington and C.F. Baillie, Phys. Rev. Lett. **68**, 962 (1992).
- [17] W. Kerler, Phys. Rev. D **47**, R1285 (1993).
- [18] W. Kerler, Phys. Rev. D **48**, 902 (1993).
- [19] M. Hennecke and U. Heyken, J. Stat. Phys. **72**, 829 (1993).
- [20] J.-S. Wang, O. Kozan and R.H. Swendsen, Phys. Rev. E **66**, 057101 (2002).
- [21] W. Klein, T. Ray and P. Tamayo, Phys. Rev. Lett. **62**, 163 (1989).
- [22] T. Ray, P. Tamayo and W. Klein, Phys. Rev. A **39**, 5949 (1989).
- [23] N. Persky, R. Ben-Av, I. Kanter and E. Domany, Phys. Rev. E **54**, 2351 (1996).
- [24] M. Jerrum, T. Luczak, A.D. Sokal and E. Vigoda, The critical behavior for the Swendsen-Wang dynamics in the mean-field approximation, in preparation.
- [25] X.-J. Li and A.D. Sokal, Phys. Rev. Lett. **63**, 827 (1989).
- [26] S. Wiseman and E. Domany, Phys. Rev. E **48**, 4080 (1993).
- [27] J. Ashkin and J. Teller, Phys. Rev. **64**, 178 (1943).
- [28] R.J. Baxter, *Exactly Solved Models in Statistical Mechanics* (Academic Press, New York, 1982).
- [29] B. Nienhuis, J. Stat. Phys. **34**, 731 (1984).
- [30] P. Di Francesco, P. Mathieu and D. Sénéchal, *Conformal Field Theory* (Springer-Verlag, New York, 1997).
- [31] G. Ossola and A.D. Sokal, Critical exponents and universal amplitude ratios in the three-dimensional Ising universality class, in preparation.
- [32] R.G. Edwards and A.D. Sokal, Phys. Rev. D **38**, 2009 (1988).
- [33] P.W. Kasteleyn and C.M. Fortuin, J. Phys. Soc. Japan **26** (Suppl.), 11 (1969).
- [34] C.M. Fortuin and P.W. Kasteleyn, Physica **57**, 536 (1972).
- [35] C.M. Fortuin, Physica **58**, 393 (1972); **59**, 545 (1972).
- [36] T.W. Anderson, *The Statistical Analysis of Time Series* (Wiley, New York, 1971).

- [37] M.B. Priestley, *Spectral Analysis and Time Series*, 2 Vols. (Academic Press, London, 1981).
- [38] N. Madras and A.D. Sokal, J. Stat. Phys. **50**, 109 (1988).
- [39] H.W.J. Blöte, L.N. Shchur and A.L. Talapov, Int. J. Mod. Phys. C **10**, 1137 (1999), cond-mat/9912005.
- [40] H.G. Ballesteros, L.A. Fernández, V. Martín-Mayor, A. Muñoz Sudupe, G. Parisi and J.J. Ruiz-Lorenzo, J. Phys. A: Math. Gen. **32**, 1 (1999), cond-mat/9805125.
- [41] M. Hasenbusch, K. Pinn and S. Vinti, Phys. Rev. B **59**, 11471 (1999), hep-lat/9806012.
- [42] M. Hasenbusch, Int. J. Mod. Phys. C **12**, 911 (2001).
- [43] D.E. Knuth, *The Art of Computer Programming*, vol. 2, 2nd ed. (Addison-Wesley, Reading, Massachusetts, 1981).
- [44] P. L'Ecuyer, Math. Comp. **68**, 249 (1999).
- [45] C. Kalle and S. Wansleben, Computer Phys. Commun. **33**, 343 (1984).
- [46] T. Filk, M. Marcu and K. Fredenhagen, Phys. Lett. B **165**, 125 (1985).
- [47] O.E. Percus and J.K. Percus, J. Comput. Phys. **77**, 267 (1988).
- [48] G. Ossola and A.D. Sokal, Systematic errors due to linear congruential pseudo-random-number generators with the Swendsen–Wang algorithm, in preparation.
- [49] E. Brézin, J. C. Le Guillou and J. Zinn-Justin, in *Phase Transitions and Critical Phenomena*, Vol. 6, ed. C. Domb and M. S. Green (Academic Press, London–New York–San Francisco, 1976).
- [50] R. da Silva, N.A. Alves and J.R. Drugowich de Felício, Phys. Lett. A **298**, 325 (2002), cond-mat/0111288.
- [51] C. Munkel, D.W. Heermann, J. Adler, M. Gofman and D. Stauffer, Physica A **193**, 540 (1993).
- [52] A. Linke, D.W. Heermann, P. Altevogt and M. Siegert, Physica A **222**, 205 (1995), cond-mat/9509115.
- [53] D. Stauffer, Physica A **244**, 344 (1997).
- [54] Z.B. Li, X.W. Liu, L. Schülke and B. Zheng, Physica A **245**, 485 (1997), cond-mat/9705234.
- [55] H.-P. Ying, L. Wang, J.-B. Zhang, M. Jiang and J. Hu, Physica A **294**, 111 (2001), cond-mat/0102500.

- [56] S. Wansleben and D.P. Landau, Phys. Rev. B **43**, 6006 (1991).
- [57] H.-O. Heuer, J. Phys. A: Math. Gen. **25**, L567 (1992).
- [58] P. Grassberger, Physica A **214**, 547 (1995).
- [59] B. Zheng, Int. J. Mod. Phys. B **12**, 1419 (1998).
- [60] A. Jaster, J. Mainville, L. Schülke and B. Zheng, J. Phys. A: Math. Gen. **32**, 1395 (1999), cond-mat/9808131.
- [61] N. Ito, K. Hukushima, K. Ogawa and Y. Ozeki, J. Phys. Soc. Japan **69**, 1931 (2000).
- [62] P. Calabrese, V. Martín-Mayor, A. Pelissetto and E. Vicari, Phys. Rev. E **68**, 016110 (2003), cond-mat/0301588.
- [63] P.C. Hohenberg and B.I. Halperin, Rev. Mod. Phys. **49**, 435 (1977).
- [64] D.W. Heermann and A.N. Burkitt, Physica A **162**, 210 (1990).

$L$	Total # iterations	Total # discarded	Lengths (and numbers) of individual runs	$\tau_{\text{int},\mathcal{E}'}$	# measurements in units of $\tau_{\text{int},\mathcal{E}'}$	CPU time ( $\mu\text{sec}/\text{spin}$ )	CPU time (years)
4	$10^8$	$10^5$	$10^8$ (1)	2.3873	$4.2 \times 10^7$	0.90	0.000
6	$10^8$	$10^5$	$10^8$ (1)	3.1054	$3.2 \times 10^7$	0.56	0.000
8	$10^8$	$10^5$	$10^8$ (1)	3.7182	$2.7 \times 10^7$	0.45	0.001
12	$10^8$	$10^5$	$10^8$ (1)	4.7469	$2.1 \times 10^7$	0.40	0.002
16	$5 \times 10^8$	$5 \times 10^5$	$10^8$ (5)	5.6180	$8.9 \times 10^7$	0.39	0.025
24	$10^8$	$10^5$	$10^8$ (1)	7.0712	$1.4 \times 10^7$	0.40	0.018
32	$2 \times 10^8$	$2 \times 10^5$	$10^8$ (2)	8.2563	$2.4 \times 10^7$	0.42	0.087
48	$3.8 \times 10^8$	$2.1 \times 10^6$	$10^8$ (2), $10^7$ (17), $5 \times 10^6$ (2)	10.2101	$3.7 \times 10^7$	0.43	0.573
64	$3.1 \times 10^8$	$2.7 \times 10^6$	$2 \times 10^7$ (12), $10^7$ (5), $2 \times 10^6$ (10)	11.7976	$2.6 \times 10^7$	0.44	1.133
96	$8.6 \times 10^7$	$1.9 \times 10^6$	$5 \times 10^6$ (17), $5 \times 10^5$ (2)	14.4677	$5.8 \times 10^6$	0.45	1.085
128	$4.8 \times 10^7$	$2.4 \times 10^6$	$2.5 \times 10^6$ (16), $10^6$ (8)	16.5379	$2.8 \times 10^6$	0.46	1.467
192	$2.9 \times 10^7$	$3.3 \times 10^6$	$10^6$ (25), $5 \times 10^5$ (8)	19.8511	$1.3 \times 10^6$	0.47	3.057
256	$4.05 \times 10^7$	$4.6 \times 10^6$	$10^6$ (35), $5 \times 10^5$ (11)	22.6743	$1.6 \times 10^6$	0.48	10.335

Table 1: Summary of our runs. The total CPU time used in these runs was approximately 17.8 years.

$L$	$\chi$		$C_H$	$\xi$	$E$	$C_1/L^d$
4	21.1944 $\pm$ 0.0033		6.6297 $\pm$ 0.0012	2.52000 $\pm$ 0.00036	0.4310438 $\pm$ 0.0000405	0.512987 $\pm$ 0.000043
6	49.0575 $\pm$ 0.0089		8.3079 $\pm$ 0.0019	3.81458 $\pm$ 0.00057	0.3881242 $\pm$ 0.0000280	0.424582 $\pm$ 0.000043
8	87.8535 $\pm$ 0.0175		9.4539 $\pm$ 0.0024	5.10153 $\pm$ 0.00080	0.3690531 $\pm$ 0.0000212	0.368769 $\pm$ 0.000042
12	197.8047 $\pm$ 0.0449		11.0562 $\pm$ 0.0032	7.66909 $\pm$ 0.00130	0.3522118 $\pm$ 0.0000140	0.300979 $\pm$ 0.000039
16	350.5792 $\pm$ 0.0388		12.2219 $\pm$ 0.0017	10.23802 $\pm$ 0.00083	0.3448934 $\pm$ 0.0000047	0.260170 $\pm$ 0.000017
24	783.1500 $\pm$ 0.2170		13.9336 $\pm$ 0.0050	15.38221 $\pm$ 0.00302	0.3385100 $\pm$ 0.0000068	0.211590 $\pm$ 0.000034
32	1382.5072 $\pm$ 0.2921		15.1928 $\pm$ 0.0042	20.52010 $\pm$ 0.00303	0.3357384 $\pm$ 0.0000035	0.182575 $\pm$ 0.000023
48	3076.1461 $\pm$ 0.5232		17.0744 $\pm$ 0.0038	30.80276 $\pm$ 0.00359	0.3333254 $\pm$ 0.0000016	0.148217 $\pm$ 0.000015
64	5420.9953 $\pm$ 1.0953		18.4697 $\pm$ 0.0049	41.08335 $\pm$ 0.00563	0.3322826 $\pm$ 0.0000013	0.127789 $\pm$ 0.000015
96	12038.7855 $\pm$ 5.1149		20.5499 $\pm$ 0.0114	61.65067 $\pm$ 0.01750	0.3313744 $\pm$ 0.0000016	0.103645 $\pm$ 0.000026
128	21193.9763 $\pm$ 13.0416		22.1551 $\pm$ 0.0179	82.20142 $\pm$ 0.03354	0.3309822 $\pm$ 0.0000016	0.089301 $\pm$ 0.000033
192	47036.4986 $\pm$ 41.9075		24.4737 $\pm$ 0.0288	123.33211 $\pm$ 0.07213	0.3306421 $\pm$ 0.0000013	0.072421 $\pm$ 0.000039
256	83001.9797 $\pm$ 66.8752		26.2767 $\pm$ 0.0280	164.74988 $\pm$ 0.08662	0.3304971 $\pm$ 0.0000008	0.062502 $\pm$ 0.000031

Table 2: Static data from the Monte Carlo simulations at the critical point of the 3-dimensional Ising model. For each lattice size ( $L$ ), we report the susceptibility ( $\chi$ ), the specific heat ( $C_H$ ), the second-moment correlation length ( $\xi$ ), the energy ( $E$ ), and the mean size of the largest cluster ( $C_1$ ). The quoted error bar corresponds to one standard deviation (i.e. confidence level  $\approx 68\%$ ).

$L$	$\tau_{\text{int},\mathcal{N}}$	$\tau_{\text{int},\mathcal{E}}$	$\tau_{\text{int},\mathcal{E}'}$	$\tau_{\text{int},\mathcal{M}^2}$	$\tau_{\text{int},\mathcal{S}_2}$
4	$2.1169 \pm 0.0018$	$2.3697 \pm 0.0021$	$2.3906 \pm 0.0022$	$2.3493 \pm 0.0021$	$2.3830 \pm 0.0022$
6	$2.7257 \pm 0.0026$	$3.0618 \pm 0.0031$	$3.1098 \pm 0.0031$	$3.0301 \pm 0.0031$	$3.0977 \pm 0.0031$
8	$3.2298 \pm 0.0033$	$3.6496 \pm 0.0040$	$3.7238 \pm 0.0041$	$3.5959 \pm 0.0039$	$3.7030 \pm 0.0041$
12	$4.0638 \pm 0.0047$	$4.6314 \pm 0.0058$	$4.7558 \pm 0.0060$	$4.5324 \pm 0.0056$	$4.7187 \pm 0.0059$
16	$4.7701 \pm 0.0027$	$5.4588 \pm 0.0033$	$5.6303 \pm 0.0034$	$5.3069 \pm 0.0031$	$5.5739 \pm 0.0034$
24	$5.9567 \pm 0.0083$	$6.8408 \pm 0.0102$	$7.0897 \pm 0.0108$	$6.5789 \pm 0.0096$	$6.9923 \pm 0.0105$
32	$6.9303 \pm 0.0074$	$7.9625 \pm 0.0090$	$8.2727 \pm 0.0096$	$7.5922 \pm 0.0084$	$8.1362 \pm 0.0094$
48	$8.5612 \pm 0.0073$	$9.8308 \pm 0.0090$	$10.2429 \pm 0.0096$	$9.2535 \pm 0.0083$	$10.0271 \pm 0.0093$
64	$9.8955 \pm 0.0101$	$11.3374 \pm 0.0124$	$11.8272 \pm 0.0132$	$10.5715 \pm 0.0112$	$11.5342 \pm 0.0127$
96	$12.1713 \pm 0.0263$	$13.8983 \pm 0.0321$	$14.5123 \pm 0.0343$	$12.7790 \pm 0.0284$	$14.0740 \pm 0.0327$
128	$13.9684 \pm 0.0438$	$15.8963 \pm 0.0533$	$16.5963 \pm 0.0567$	$14.4798 \pm 0.0462$	$16.0373 \pm 0.0540$
192	$16.8861 \pm 0.0778$	$19.0981 \pm 0.0933$	$19.9312 \pm 0.0996$	$17.0821 \pm 0.0790$	$19.0814 \pm 0.0933$
256	$19.3990 \pm 0.0813$	$21.8291 \pm 0.0969$	$22.7669 \pm 0.1034$	$19.4148 \pm 0.0814$	$21.7656 \pm 0.0967$

Table 3: Autocorrelation times for the Swendsen–Wang algorithm at the critical point of the 3-dimensional Ising model. For each lattice size ( $L$ ), we report the integrated autocorrelation time for the bond occupation ( $\tau_{\text{int},\mathcal{N}}$ ), the energy ( $\tau_{\text{int},\mathcal{E}}$ ), the nearest-neighbor connectivity ( $\tau_{\text{int},\mathcal{E}'}$ ), the squared magnetization ( $\tau_{\text{int},\mathcal{M}^2}$ ), and the mean-square cluster size ( $\tau_{\text{int},\mathcal{S}_2}$ ). The quoted error bar corresponds to one standard deviation (i.e. confidence level  $\approx 68\%$ ).

$L$	$\tau_{\text{int},\mathcal{S}_0}$	$\tau_{\text{int},\mathcal{C}_1}$	$\tau_{\text{int},\mathcal{C}_2}$	$\tau_{\text{int},\mathcal{C}_3}$
4	$2.0347 \pm 0.0019$	$2.2994 \pm 0.0020$	$1.1843 \pm 0.0010$	$1.4474 \pm 0.0014$
6	$2.5473 \pm 0.0026$	$2.9784 \pm 0.0029$	$1.3890 \pm 0.0013$	$1.7324 \pm 0.0018$
8	$2.9917 \pm 0.0033$	$3.5488 \pm 0.0039$	$1.5639 \pm 0.0015$	$1.9720 \pm 0.0022$
12	$3.7408 \pm 0.0046$	$4.5025 \pm 0.0055$	$1.8564 \pm 0.0020$	$2.3786 \pm 0.0029$
16	$4.3847 \pm 0.0026$	$5.3001 \pm 0.0031$	$2.0973 \pm 0.0011$	$2.7099 \pm 0.0016$
24	$5.4764 \pm 0.0082$	$6.6205 \pm 0.0097$	$2.4807 \pm 0.0031$	$3.2554 \pm 0.0046$
32	$6.3760 \pm 0.0072$	$7.6876 \pm 0.0086$	$2.7875 \pm 0.0026$	$3.6901 \pm 0.0039$
48	$7.8999 \pm 0.0072$	$9.4380 \pm 0.0085$	$3.2661 \pm 0.0024$	$4.3843 \pm 0.0037$
64	$9.1455 \pm 0.0100$	$10.8384 \pm 0.0116$	$3.6451 \pm 0.0031$	$4.9386 \pm 0.0049$
96	$11.2938 \pm 0.0262$	$13.1816 \pm 0.0297$	$4.2519 \pm 0.0074$	$5.8452 \pm 0.0120$
128	$12.9878 \pm 0.0439$	$14.9924 \pm 0.0487$	$4.7240 \pm 0.0118$	$6.5409 \pm 0.0193$
192	$15.7728 \pm 0.0783$	$17.8138 \pm 0.0842$	$5.4151 \pm 0.0194$	$7.5908 \pm 0.0320$
256	$18.1480 \pm 0.0822$	$20.2905 \pm 0.0870$	$6.0248 \pm 0.0193$	$8.5341 \pm 0.0324$

Table 4: Autocorrelation times for the Swendsen–Wang algorithm at the critical point of the 3-dimensional Ising model. For each lattice size ( $L$ ), we report the integrated autocorrelation time for the number of clusters ( $\tau_{\text{int},\mathcal{S}_0}$ ) and for the sizes of the three largest clusters ( $\tau_{\text{int},\mathcal{C}_i}$  for  $i = 1, 2, 3$ ). The quoted error bar corresponds to one standard deviation (i.e. confidence level  $\approx 68\%$ ).

Exponent	Estimate	$L_{\min}$	$\chi^2$ (DF, CL)
$z_{\text{int}, \mathcal{N}}$	$0.4745 \pm 0.0044$	96	0.263 (2 DF, 87.7%)
$z_{\text{int}, \mathcal{E}}$	$0.4599 \pm 0.0046$	96	0.338 (2 DF, 84.4%)
$z_{\text{int}, \mathcal{E}'}$	$0.4588 \pm 0.0047$	96	0.352 (2 DF, 83.8%)
$z_{\text{int}, \mathcal{M}^2}$	$0.4245 \pm 0.0044$	96	1.641 (2 DF, 44.0%)
$z_{\text{int}, \mathcal{S}_2}$	$0.4432 \pm 0.0046$	96	1.126 (2 DF, 57.0%)
$z_{\text{int}, \mathcal{S}_0}$	$0.4832 \pm 0.0047$	96	0.082 (2 DF, 96.0%)
$z_{\text{int}, \mathcal{C}_1}$	$0.4384 \pm 0.0045$	96	0.971 (2 DF, 61.5%)
$z_{\text{int}, \mathcal{C}_2}$	$0.3537 \pm 0.0034$	96	2.786 (2 DF, 24.8%)
$z_{\text{int}, \mathcal{C}_3}$	$0.3836 \pm 0.0040$	96	1.975 (2 DF, 37.2%)

Table 5: Numerical estimates for the dynamic critical exponents of the 3-dimensional Ising model, based on least-squares fits with the specified  $L_{\min}$ . The quoted error bar corresponds to one standard deviation (i.e. confidence level  $\approx 68\%$ ).

$L$	$A_{\mathcal{N}}$	$\tau_{\text{exp},\mathcal{N}}$	$A_{\mathcal{E}}$	$\tau_{\text{exp},\mathcal{E}}$	$A_{\mathcal{E}'}$	$\tau_{\text{exp},\mathcal{E}'}$	$A_{\mathcal{M}^2}$	$\tau_{\text{exp},\mathcal{M}^2}$	$A_{\mathcal{S}_2}$	$\tau_{\text{exp},\mathcal{S}_2}$
4	0.8496	2.3588	0.9843	2.3628	0.9975	2.3611	0.9738	2.3604	0.9937	2.3602
6	0.8372	3.1071	0.9704	3.1059	0.9895	3.1080	0.9561	3.1063	0.9845	3.1078
8	0.8284	3.7396	0.9622	3.7414	0.9875	3.7407	0.9440	3.7411	0.9810	3.7397
12	0.8157	4.8034	0.9524	4.8069	0.9844	4.8060	0.9275	4.8062	0.9748	4.8065
16	0.8028	5.7303	0.9406	5.7284	0.9755	5.7308	0.9090	5.7305	0.9638	5.7323
24	0.7919	7.2722	0.9283	7.2692	0.9682	7.2687	0.8899	7.2575	0.9548	7.2621
32	0.7857	8.5472	0.9196	8.5443	0.9615	8.5429	0.8728	8.5374	0.9451	8.5379
48	0.7827	10.6314	0.9112	10.6380	0.9548	10.6364	0.8532	10.6385	0.9333	10.6400
64	0.7785	12.3751	0.9037	12.3777	0.9473	12.3835	0.8365	12.4059	0.9218	12.4023
96	0.7709	15.3193	0.8879	15.3373	0.9326	15.3276	0.8126	15.3481	0.9041	15.3353
128	0.7748	17.6210	0.8884	17.6409	0.9316	17.6424	0.8043	17.6836	0.8987	17.6729
192	0.7782	21.2902	0.8867	21.2979	0.9289	21.3083	0.7949	21.2413	0.8933	21.2720
256	0.7679	24.6645	0.8725	24.6212	0.9133	24.6273	0.7728	24.6522	0.8729	24.6519

Table 6: Estimates of the amplitude  $A_{\mathcal{O}}$  and the exponential autocorrelation time  $\tau_{\text{exp},\mathcal{O}}$  for the observables  $\mathcal{N}$ ,  $\mathcal{E}$ ,  $\mathcal{E}'$ ,  $\mathcal{M}^2$  and  $\mathcal{S}_2$ .

$L$	$A_{\mathcal{S}_0}$	$\tau_{\text{exp},\mathcal{S}_0}$	$A_{\mathcal{C}_1}$	$\tau_{\text{exp},\mathcal{C}_1}$	$A_{\mathcal{C}_2}$	$\tau_{\text{exp},\mathcal{C}_2}$	$A_{\mathcal{C}_3}$	$\tau_{\text{exp},\mathcal{C}_3}$
4	0.7991	2.3582	0.9479	2.3499	0.3298	2.3284	0.4858	2.3399
6	0.7631	3.1055	0.9342	3.0971	0.3028	3.0851	0.4494	3.0761
8	0.7500	3.7358	0.9297	3.7252	0.2931	3.7079	0.4318	3.7036
12	0.7361	4.7983	0.9207	4.7843	0.2781	4.7952	0.4108	4.7733
16	0.7248	5.7269	0.9078	5.7042	0.2698	5.7093	0.3970	5.6844
24	0.7165	7.2712	0.8936	7.2358	0.2612	7.2010	0.3809	7.2192
32	0.7131	8.5471	0.8838	8.4986	0.2520	8.5026	0.3710	8.4798
48	0.7139	10.6296	0.8704	10.5925	0.2425	10.6074	0.3582	10.5656
64	0.7125	12.3728	0.8585	12.3428	0.2353	12.3740	0.3471	12.3565
96	0.7085	15.3250	0.8406	15.2511	0.2250	15.3425	0.3358	15.2290
128	0.7154	17.6157	0.8335	17.5967	0.2214	17.6720	0.3301	17.5485
192	0.7218	21.2930	0.8265	21.2023	0.2146	21.3083	0.3242	21.0661
256	0.7139	24.6895	0.8078	24.5465	0.2076	24.7020	0.3105	24.6323

Table 7: Estimates of the amplitude  $A_{\mathcal{O}}$  and the exponential autocorrelation time  $\tau_{\text{exp},\mathcal{O}}$  for the observables  $\mathcal{S}_0$ ,  $\mathcal{C}_1$ ,  $\mathcal{C}_2$  and  $\mathcal{C}_3$ .



$L$	$A_{\mathcal{N}}$	$R_{\mathcal{N}}$	$A_{\mathcal{E}}$	$R_{\mathcal{E}}$	$A_{\mathcal{E}'}$	$R_{\mathcal{E}'}$	$A_{\mathcal{M}^2}$	$R_{\mathcal{M}^2}$	$A_{\mathcal{S}_2}$	$R_{\mathcal{S}_2}$
4	0.8496	0.8834	0.9843	0.9889	0.9975	0.9976	0.9738	0.9804	0.9937	0.9945
6	0.8372	0.8695	0.9704	0.9767	0.9895	0.9920	0.9561	0.9666	0.9845	0.9882
8	0.8284	0.8583	0.9622	0.9699	0.9875	0.9896	0.9440	0.9556	0.9810	0.9841
12	0.8157	0.8425	0.9524	0.9602	0.9844	0.9860	0.9275	0.9397	0.9748	0.9783
16	0.8028	0.8303	0.9406	0.9501	0.9755	0.9800	0.9090	0.9237	0.9638	0.9702
24	0.7919	0.8182	0.9283	0.9397	0.9682	0.9738	0.8899	0.9037	0.9548	0.9605
32	0.7857	0.8103	0.9196	0.9310	0.9615	0.9673	0.8728	0.8877	0.9451	0.9513
48	0.7827	0.8043	0.9112	0.9236	0.9548	0.9623	0.8532	0.8693	0.9333	0.9420
64	0.7785	0.7987	0.9037	0.9150	0.9473	0.9546	0.8365	0.8532	0.9218	0.9309
96	0.7709	0.7938	0.8879	0.9064	0.9326	0.9465	0.8126	0.8334	0.9041	0.9179
128	0.7748	0.7915	0.8884	0.9008	0.9316	0.9405	0.8043	0.8205	0.8987	0.9088
192	0.7782	0.7923	0.8867	0.8961	0.9289	0.9352	0.7949	0.8015	0.8933	0.8953
256	0.7679	0.7876	0.8725	0.8863	0.9133	0.9243	0.7728	0.7882	0.8729	0.8837

Table 8: Estimates of the amplitude  $A_{\mathcal{O}}$  and the ratio  $R_{\mathcal{O}} = \tau_{\text{int},\mathcal{O}}/\bar{\tau}_{\text{exp}}$  for the observables  $\mathcal{N}$ ,  $\mathcal{E}$ ,  $\mathcal{E}'$ ,  $\mathcal{M}^2$  and  $\mathcal{S}_2$ .

$L$	$A_{\mathcal{S}_0}$	$R_{\mathcal{S}_0}$	$A_{\mathcal{C}_1}$	$R_{\mathcal{C}_1}$	$A_{\mathcal{C}_2}$	$R_{\mathcal{C}_2}$	$A_{\mathcal{C}_3}$	$R_{\mathcal{C}_3}$
4	0.7991	0.8491	0.9479	0.9596	0.3298	0.4942	0.4858	0.6040
6	0.7631	0.8126	0.9342	0.9501	0.3028	0.4431	0.4494	0.5527
8	0.7500	0.7950	0.9297	0.9431	0.2931	0.4156	0.4318	0.5241
12	0.7361	0.7756	0.9207	0.9335	0.2781	0.3849	0.4108	0.4931
16	0.7248	0.7632	0.9078	0.9225	0.2697	0.3650	0.3970	0.4717
24	0.7165	0.7522	0.8936	0.9094	0.2612	0.3407	0.3809	0.4472
32	0.7131	0.7455	0.8838	0.8989	0.2520	0.3259	0.3710	0.4315
48	0.7139	0.7422	0.8704	0.8867	0.2425	0.3068	0.3582	0.4119
64	0.7125	0.7381	0.8585	0.8748	0.2353	0.2942	0.3471	0.3986
96	0.7085	0.7366	0.8406	0.8597	0.2250	0.2773	0.3358	0.3812
128	0.7154	0.7360	0.8335	0.8496	0.2214	0.2677	0.3301	0.3706
192	0.7218	0.7401	0.8265	0.8358	0.2146	0.2541	0.3242	0.3562
256	0.7139	0.7368	0.8078	0.8238	0.2076	0.2446	0.3105	0.3465

Table 9: Estimates of the amplitude  $A_{\mathcal{O}}$  and the ratio  $R_{\mathcal{O}} = \tau_{\text{int},\mathcal{O}}/\bar{\tau}_{\text{exp}}$  for the observables  $\mathcal{S}_0$ ,  $\mathcal{C}_1$ ,  $\mathcal{C}_2$  and  $\mathcal{C}_3$ .

Model	$\alpha/\nu$	$\beta/\nu$	$\gamma/\nu$	$z_G$	$z_{\text{KRT}}^{(\text{lower})}$	$z_{\text{SW}}$	$z_{\text{KRT}}^{(\text{upper})}$
$d = 1$ , all $q$	—	0	1	2	0	0	0
$d = 2$ Ising	$0 (\times \log)$	$1/8$	$7/4$	2.16(2)	0.29(2)	0.222(7) [10]	0.41(2)
$d = 2$ , $q = 3$	$2/5$	$2/15$	$26/15$	2.19(2)	0.33(2)	0.514(6) [11]	0.46(2)
$d = 2$ , $q = 4$	$1 (\times \log^{-3/2})$	$1/8 (\times \log^{1/16})$	$7/4 (\times \log^{-1/8})$	2.25(6)	0.38(6)	$1 (\times \log^{??})$ [13]	0.50(6)
$d = 3$ Ising	0.1756(25)	0.5183(4)	1.9634(8)	2.04(4)	0.46(4)	0.46(3) [this work]	0.73(4)
$d = 4$ Ising	$0 (\times \log^{1/3})$	$1 (\times \log^{1/6})$	2	2	2/3	$1 (\times \log^{??})$	1

Table 10: Dynamic critical exponent  $z_{\text{int},\mathcal{E}'}$  of the Swendsen–Wang algorithm for various Potts models, compared to the exponents arising in the theoretical frameworks of Li and Sokal [25], Klein, Ray and Tamayo [21], and Coddington and Baillie [16]. Static critical exponents  $\alpha/\nu$ ,  $\beta/\nu$  and  $\gamma/\nu$  are exact values for the  $d = 1$  and  $d = 2$  models [13, 28–30] and for  $d = 4$  Ising [49], and are the best currently available numerical estimates for  $d = 3$  Ising [41]. Exponent  $z_G$  for Glauber dynamics is taken from [50, Table 1] for the  $d = 2$  models (see also [51–55]), from [51, 53, 56–62] for  $d = 3$  Ising, and from [63] for  $d = 4$  Ising.

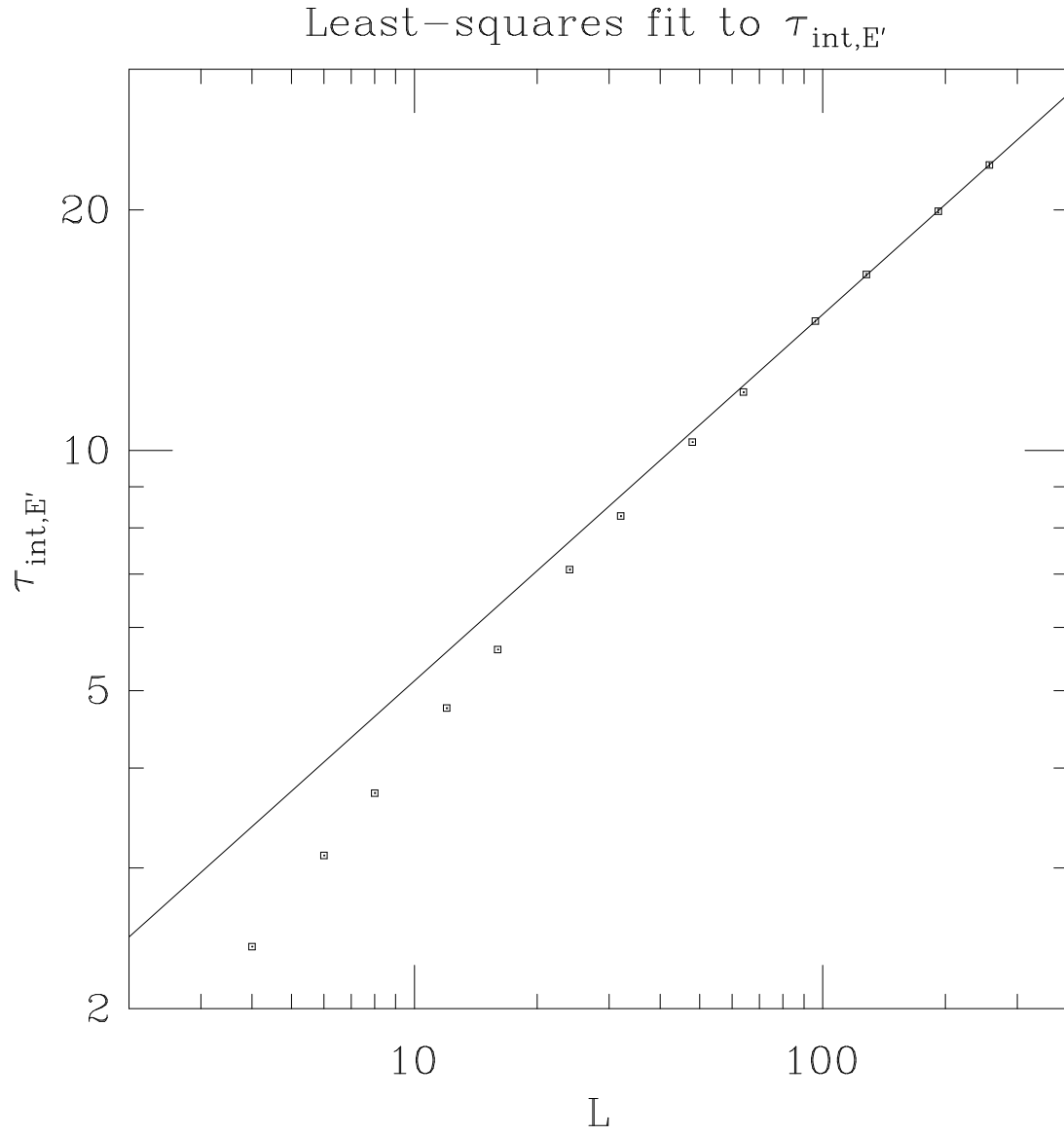


Figure 1:  $\tau_{\text{int},E'}$  versus  $L$ . Error bars are in all cases smaller than the plot symbol. The least-squares fit line is  $\tau_{\text{int},E'} = 1.78861L^{0.45878}$  and is obtained for  $L_{\text{min}} = 96$ .

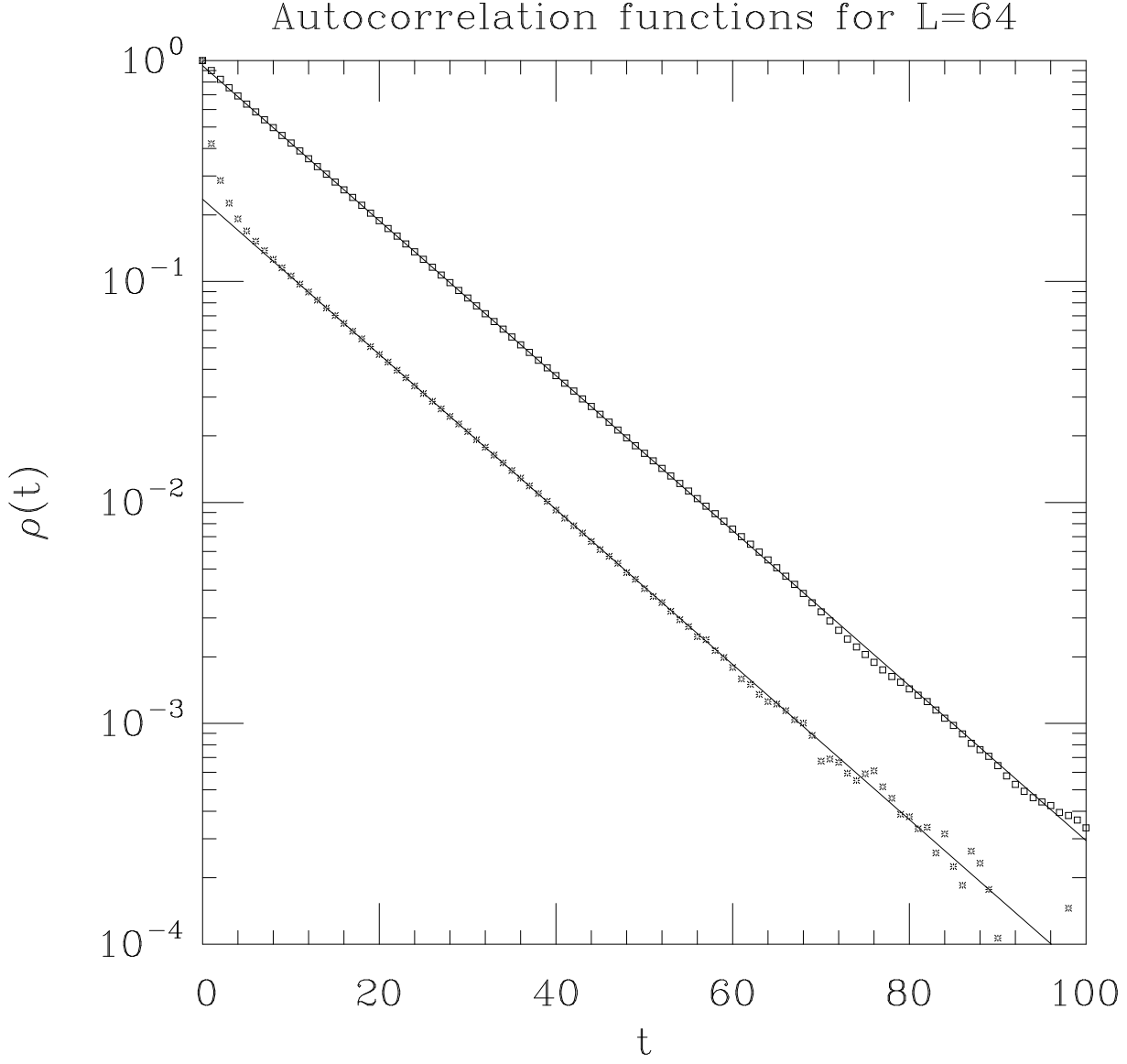


Figure 2: Autocorrelation functions  $\rho_{\mathcal{O}\mathcal{O}}(t)$  for observables  $\mathcal{O} = \mathcal{E}'$  ( $\square$ ) and  $\mathcal{C}_2$  ( $*$ ) at  $L = 64$ . We have also depicted the straight-line fits corresponding to  $\tau_{\text{exp},\mathcal{O}}$ .

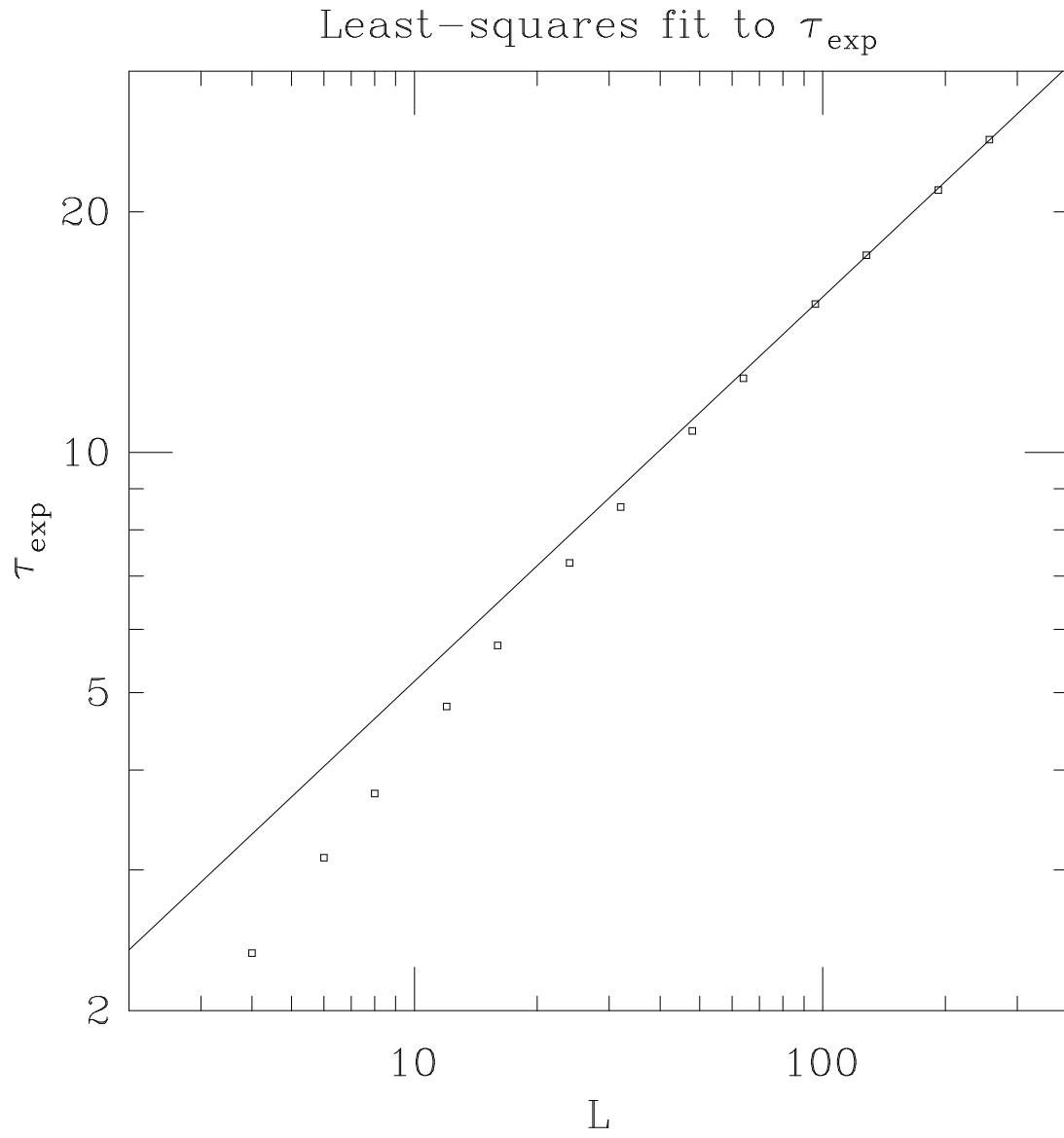


Figure 3:  $\tau_{\text{exp}}$  versus  $L$ . The least-squares fit line is  $\tau_{\text{exp}} = 1.706L^{0.481}$  and is obtained for  $L_{\min} = 96$ . The value of  $\tau_{\text{exp}}$  is taken from  $\tau_{\text{exp},\mathcal{E}'}$  in Table 6.

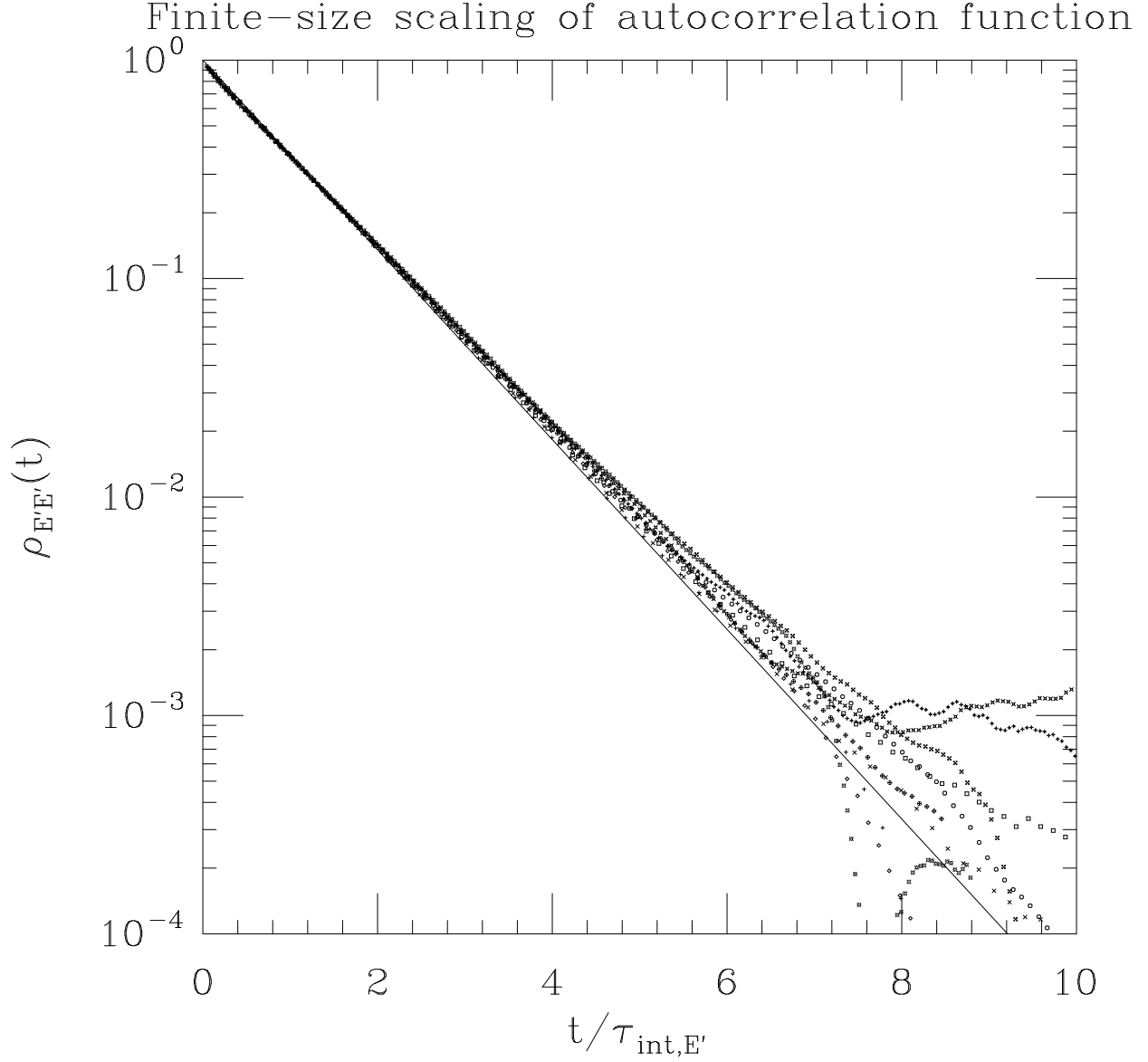


Figure 4:  $\rho_{\mathcal{E}'\mathcal{E}'}(t)$  versus  $t/\tau_{\text{int},\mathcal{E}'}$  for  $12 \leq L \leq 256$ . The different symbols denote the different lattice sizes:  $L = 12$  (+),  $L = 16$  ( $\times$ ),  $L = 24$  ( $\square$ ),  $L = 32$  ( $\diamond$ ),  $L = 48$  ( $\circ$ ),  $L = 64$  ( $\oplus$ ),  $L = 96$  ( $\otimes$ ),  $L = 128$  ( $\boxtimes$ ),  $L = 192$  ( $\star$ ),  $L = 256$  (\*). For comparison, we have also depicted the line corresponding to the pure exponential  $\rho_{\mathcal{E}'\mathcal{E}'}(t) = \exp(-t/\tau_{\text{int},\mathcal{E}'})$ .

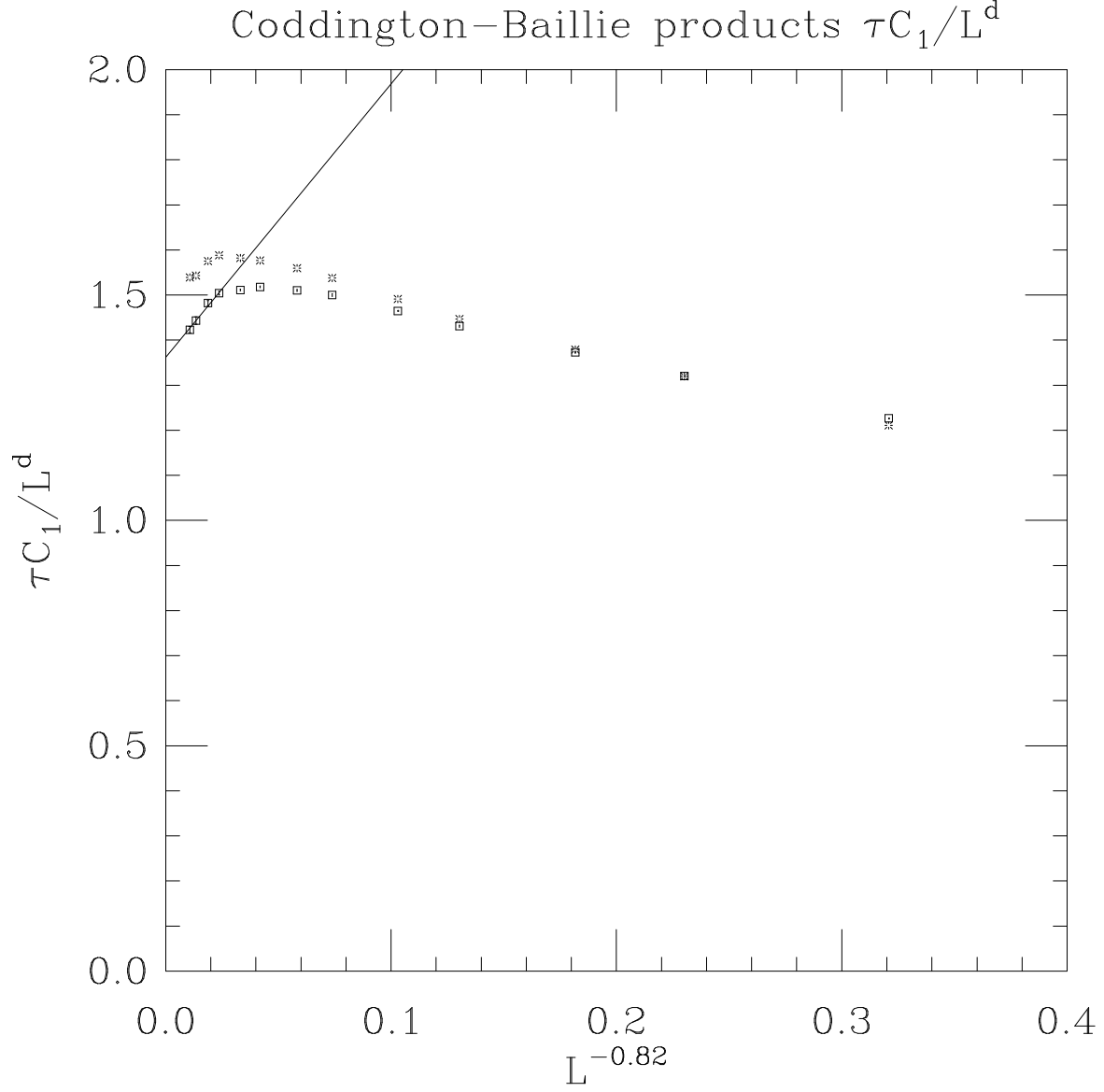


Figure 5: The Coddington–Baillie products  $\tau_{\text{int}, \epsilon'} C_1/L^d$  (□ with triangle-inequality error bars) and  $\tau_{\text{exp}, \epsilon'} C_1/L^d$  (\*) without error bars) versus  $L^{-0.82}$ . The least-squares fit line is  $\tau_{\text{int}, \epsilon'} C_1/L^d = 1.362 + 6.064L^{-0.82}$  and is obtained for  $L_{\text{min}} = 96$ .